Active and STAR-RIS Assisted MIMO ISAC Systems with SWIPT

Jetti Yaswanth, Prajwalita Saikia, *Member, IEEE*, Keshav Singh, *Member, IEEE*, Yun Hee Kim, *Senior Member, IEEE*, and Trung Q. Duong, *Fellow, IEEE*

***Abstract*—As an innovative framework for sustainable communication within next-generation networks, reconfigurable intelligent surfaces (RISs) have developed potential transformation in improving simultaneous wireless information and power transfer (SWIPT). Alongside SWIPT, integrated sensing and communication (ISAC) has gained significant attention for its ability to combine communication and sensing functionalities within the same infrastructure, optimizing resource utilization and improving system performance. In this paper, we propose a framework that integrates an active (A-RIS) and simultaneous transmitting and reflecting RIS (STAR-RIS) assisted multiple-input multiple-output (MIMO) technology for SWIPT in an ISAC system. The system consists of an A-RIS, a STAR-RIS, a dual functional base station (DFBS), a group of reflection and transmission communication users (CUs) and reflection and transmission energy receiving devices (EDs), sensing targets simultaneously with the aid of RIS. We formulate an optimization problem to maximize the target rate while balancing the communication rate under energy harvesting (EH) constraints, and phase-shits constraints. It implies the trade-offs between target sensing accuracy and communication performance, demonstrating the potential of RIS to enhance system capabilities in diverse ISAC scenarios. The optimization problem and its constraints are inherently non-convex due to the high coupling between variables. Consequently, we employ the minimum mean square error method to address the non-convex nature of the problem. Thereby, it simplifies the problem by transforming it into a more manageable form and then applying an alternating optimization framework. This framework addresses the design of beamforming challenges at both the DFBS and the RIS (A-RIS/STAR-RIS) separately, by solving them iteratively using general approximation techniques. The analysis highlights the advantages of the proposed ARIS and STAR-RIS assisted SWIPT for ISAC framework over conventional RIS by achieving performance gain of 12-15%.**

***Index Terms*—Active-reconfigurable intelligent surface (A-RIS), green communication, integrated sensing and communication, multiple input multiple output, simultaneous transmitting and reflecting RIS (STAR-RIS), simultaneous wireless information and power transfer.**

I. Introduction

Integrated sensing and communication (ISAC) is a paradigm shift in wireless communication that merges the functionalities of sensing and communication into a single platform [1]. This convergence is expected to play a pivotal role in the development of 6G networks and the Internet-of-Things (IoT) [2]. However, this integration is driven by the need for higher spectral efficiency, improved energy utilization, and advanced capabilities in the rapidly evolving world of the IoT, smart cities, and autonomous systems [3]. Nevertheless, 6G networks are designed to accommodate an extensive array of devices, encompassing smartphones, sensors, IoT devices, and robotic systems, thereby facilitating ISAC [4], [5]. Early works on ISAC initially concentrated on separating communication and sensing resources to minimize interference, using techniques like time-division, spatial-division, and frequency-division ISAC [6], [7]. Although these methods are easier to implement in hardware, they are limited by low spectrum and energy efficiency. To overcome these limitations, three types of fully unified ISAC waveform designs have been introduced: sensing-centric design, communication-centric design, and joint design.

By integrating the ISAC with with the simultaneous wireless information and power transfer (SWIPT) system, we can have a privilege to serve both the ground users and sensing targets on ground, sea and air. However the design is more complex in some cases like we need to provide the user fairness between both the systems. The SWIPT is a technology where DFBS transmits the signal to the communication users and energy receivers simultaneously [8]. We define the user only receives the information from the DFBS are termed as communication users and devices which consumes the energy from the signals are termed as energy devices/energy receivers. In general, these these energy receivers are low power devices which requires minimal amount if the power to satisfy the QoS [9]. However, there will a few disadvantages using these systems like fading effect in scenarios like high interference region or receivers located in the far region from the DFBS, which requires more power to stratify the required QoS. To guarantee

The work of K. Singh was supported by the National Science and Technology Council of Taiwan under Grant NSTC 112-2221-E-110-038-MY3. The work of Y. H. Kim was supported by the National Research Foundation of Korea (NRF) under Grant NRF-2021R1A2C1005869 and by the Institute of Information & Communications Technology Planning & Evaluation (IITP) under the Information Technology Research Center (ITRC) support program IITP-2024-2021-0-02046, with funding from the Ministry of Science and ICT (MSIT), Korea. The work of T. Q. Duong was supported by Canada Excellence Research Chairs Program CERC-2022-00109. (*Corresponding authors: Keshav Singh and Yun Hee Kim.*)

J. Yaswanth and P. Saikia are with the Institute of Communications Engineering, National Sun Yat-sen University, Kaohsiung, Taiwan (E-mail: yaswanthj98@gmail.com, mitalisaikiajist@gmail.com).

K. Singh is with the Institute of Communications Engineering, National Sun Yat-sen University, Kaohsiung 80424, Taiwan, and also with the Department of Electronic Engineering, Kyung Hee University, Yongin-si, Gyeonggi-do 17104, South Korea (E-mail: keshav.singh@mail.nsysu.edu.tw).

Y. H. Kim is with the Department of Electronic Engineering and also with the Department of Electronics and Information Convergence Engineering, Kyung Hee University, Yongin 17104, South Korea (E-mail: yheekim@khu.ac.kr).

T. Q. Duong is with the Faculty of Engineering and Applied Science, Memorial University, St. John's, NL A1C 5S7, Canada and also with the School of Electronics, Electrical Engineering and Computer Science, Queen's University Belfast, BT7 1NN Belfast, U.K. (E-mail: tduong@mun.ca).

the sustainable functionality of these devices, particularly low-power IoT devices, the incorporation of wireless power transfer (WPT) within 6G networks is proposed [10], [11]. Through the amalgamation of ISAC and WPT, 6G has the potential to evolve into a multifunctional wireless network characterized by integrated sensing, communication, and power provision at the air interface. With their recent technological progressions, it is anticipated that forthcoming 6G networks will amalgamate both SWIPT and ISAC, thereby progressing towards novel multifunctional wireless systems that can concurrently deliver sensing, communication, and power provisioning capabilities [11].

To accommodate a vast number of IoT devices spread across various locations, it is crucial to expand the reach and coverage of current wireless networks. Reconfigurable intelligent surfaces (RIS) can overcome environmental barriers by creating virtual line-of-sight (LoS) links, significantly increasing the coverage area and enabling more IoT devices to be supported [12]. An RIS consists of passive metasurfaces that reflect incoming signals without the need for an independent power source [13], [14]. It provide a promising solution to this challenge by creating dependable virtual connections between the dual-function radar-communications (DFRC) base station (BS) and the sensing targets. However, traditional beamforming methods for passive RIS experience significant signal degradation due to the multiplicative fading effect, leading to potential detection issues at the receiver. In contrast, active RIS (A-RIS) can mitigate this problem by amplifying the transmitted signals, although this comes with increased energy consumption due to the amplification process [15], [16]. Recent scholarly contributions have demonstrated that the A-RIS yields markedly enhanced performance in communication systems operating under equivalent power constraints in comparison with conventional RIS [17]. Furthermore, the A-RIS has attracted considerable scholarly interest in the domain of sensing-related applications, encompassing radar detection and localization [18]. In scenarios wherein the A-RIS is utilized to create a virtual connection between the DFRC BS and the intended recipient, a signal that would conventionally experience substantial attenuation can be enhanced on two occasions using the same active RIS panel, a phenomenon we refer to as multiple-self-reflection.

Recently, the simultaneous transmitting and reflecting reconfigurable intelligent surface (STAR-RIS) has been developed as a dual-sided RIS, allowing it to retransmit signals to areas behind the surface, thus providing 360-degree coverage for all users. One portion of the signal, known as the reflected signal, is directed back into the same area as the incoming signal, referred to as the reflection space. Meanwhile, the other portion, called the transmitted signal, is sent to the area opposite to the incoming signal, known as the transmission space. By enabling interaction on both sides of the RIS, STAR-RIS adds an extra degree of freedom (DoF) and improves the energy efficiency compared to traditional one-sided RIS systems [19], [20]. The STAR-RIS helps to serve the users located on the blind spot from the BS and provide the extra degree of freedom.

A. Related Works

The integration of RIS into communication and sensing systems has been a prominent research focus due to its potential to significantly enhance performance metrics such as data rates, energy efficiency, and sensing accuracy. Various architectures and optimization techniques have been proposed to exploit the advantages of RIS. Active RIS systems were explored in [21], where the authors demonstrated their ability to achieve rate maximization in ISAC systems. The study focuses on maximizing the secure rate by providing low-complexity algorithms such as Successive Convex Approximation (SCA) and Majorization-Minimization (MM). Similarly, [22] investigated Intelligent Omni-surfaces, which optimize beamforming, phase, and amplitude settings to minimize self-interference, thereby achieving significant rate improvements. The STAR-RIS framework has gained significant attention in recent years. In [23], secrecy rate maximization was addressed for STAR-RIS, while works like [24] and [25] optimized sum throughput. Moreover, dual Passive RIS systems were studied in [9], where the focus was on maximizing the sum rate, and in [26], where the goal was to achieve maximum Signal-to-Noise Ratio (SNR) through similar approaches. Improving beam patterns to maximize the minimum performance of the system was the key contribution of [27]. In another study [8], Weighted Sum-Rate (WSR) optimization was addressed using Passive RIS systems. Further advancements in Active RIS systems for rate maximization were proposed in [28], showcasing the growing interest in their potential to enhance wireless network performance.

Beyond communication performance, RIS has been integrated into energy-efficient and sensing-centric systems. For instance, in [9], the authors investigated a RIS-aided cell-free MIMO network, utilizing alternating optimization techniques such as Alternating Direction Method of Multipliers (ADMM) and Successive Convex Approximation (SCA). These approaches addressed energy harvesting and RIS reflection constraints, enabling the system to maximize WSR under power constraints. Similarly, [29] introduced a Block Coordinate Descent (BCD)-based alternating optimization algorithm, which simultaneously optimized the reflection coefficients of the RIS and task allocation to maximize energy storage in RIS-assisted SWIPT and mobile edge computing-enabled networks. The potential of integrating SWIPT systems with RIS has also been explored extensively. SWIPT uses the same wireless signals to simultaneously transmit information to Information Decoding (ID) receivers and provide energy to Energy Harvesting (EH) receivers [30]. This dual functionality is further enhanced when combined with ISAC (Integrated Sensing and Communication) systems. Such integration creates multi-functional wireless systems capable of delivering sensing, communication, and power transfer simultaneously [31], [32]. These systems are particularly beneficial for IoT applications like smart cities and industrial automation, where millions of devices can be supported with sustainable power for uplink communication while enabling base stations to perform localization and send control data [33]. In [31], a significant advancement was outlined by integrating sensing,

TABLE I: Comparison with existing works

Papers	ISAC	MIMO	SWIPT	RIS	Performance metric
[21]	✓	X	X	Active-RIS	rate-maximization
[22]	X	X	X	Intelligent Omni-surface	rate-maximization
[23]	X	✓	X	STAR-RIS	secrecy rate maximization problem
[9]	X	✓	✓	Dual Passive RISs	Sum-rate maximization
[8]	X	✓	✓	Passive RIS	Sum-rate maximization
[42]	✓	X	X	X	Energy Efficiency maximization
[39]	✓	X	X	Passive RIS	maximize SNR
[26]	✓	X	X	Passive RIS	maximize the minimum beam pattern
[27]	X	✓	X	Passive RIS	Weighted Sum-rate
[25]	X	X	X	STAR-RIS	worst-case secrecy rate
[24]	X	X	X	STAR-RIS	sum throughput
[43]	X	X	X	STAR-RIS	sum throughput
[28]	X	X	X	Active-RIS	rate maximization
Our Work	✓	✓	✓	Active-RIS & STAR-RIS	Sum-rate maximization

communication, and power transfer in wireless systems while addressing associated performance trade-offs and optimization strategies. Another study [34] focused on the deployment of multiple network-in-a-box (NIBs) to maximize total network throughput, supporting both conventional broadband and IoT-sensed data. In [35], the integration of SWIPT with ISAC was explored to handle both communication and sensing tasks simultaneously, considering hardware impairments, channel estimation errors, and imperfect interference cancellation.

The integration of RIS with ISAC systems has been studied under two primary scenarios [36]–[38]. In the first scenario, RIS is used exclusively to enhance communication performance, while sensing relies on direct transceiver-target links. In the second scenario, RIS is leveraged to improve radar sensing capabilities by creating a virtual link between the base station (BS) and the target. Works such as [26], [39] focused on optimizing RIS beampatterns to direct more power toward the target for enhanced sensing resolution. However, the compounded path loss due to multiplicative fading across four-hop links significantly limits sensing resolution. To mitigate this issue, advanced RIS architectures have been proposed, demonstrating the potential to enhance both communication and sensing simultaneously. For example, integrating SWIPT into RIS-enabled systems can efficiently manage energy harvesting and information transmission for communication users (CUs) while improving the accuracy of target sensing. The role of RIS in optimizing passive and active beamforming at the Dual-Function Radar-Communication (DFRC) BS ensures improved spectral and energy efficiency. Such solutions are promising for future wireless networks with high demands for both sensing and communication [40], [41].

B. Motivation and Contribution:

In this paper, we aim to explore the dual RIS ISAC-aided SWIPT systems, an area that has not been extensively studied in the existing literature. As highlighted in Table I, the integration of RIS in ISAC-aided SWIPT systems offers several advantages, particularly in maximizing the sum-rate of the communication system under the constraints imposed by sensing interference. The STAR-RIS plays a crucial role in this system, serving users located in the blind zones of the Dual-Function Base Station (DFBS). However, none of the previous studies have addressed the dual RIS setup in ISAC-aided SWIPT systems, which forms the primary focus of our research. The core challenge in this work is to maximize the sum-rate while ensuring energy harvesting and sensing constraints are satisfied, all within the limitations of the available transmit power. The RISs used in our system play a key role by improving signal quality in situations where direct channel signals are weak, without consuming any additional power. This significantly enhances the overall system performance. Previous studies on similar topics often rely on tools like CVX to solve the formulated problems, but these approaches do not lead to closed-form solutions. In contrast, this paper aims to offer a near-optimal solution with lower complexity, addressing the challenges of sum-rate maximization under the aforementioned constraints. Additionally, the proposed framework investigates the performance of ISAC-aided SWIPT systems, shedding light on the interplay between communication and sensing functions. By integrating ISAC with SWIPT systems, we emphasize the need to allocate sufficient power for both communication and sensing tasks. This is particularly crucial when considering the potential of RIS-enhanced SWIPT ISAC systems. These systems can incorporate A-RIS for precise sensing and STAR-RIS for optimized communication and energy harvesting, thus creating a unified framework for secure, energy-efficient, and intelligent networking. Through this exploration, we highlight the promise of RIS-enhanced SWIPT ISAC systems in advancing the performance of next-generation wireless networks. By leveraging the combined strengths of A-RIS for sensing and STAR-RIS for communication and energy harvesting, our methodology offers a comprehensive approach to achieve seamless, secure, and efficient operations in modern wireless networks.

Inspired by the aforementioned context, in this work, we present a MIMO system for novel ISAC by proposing an RIS-aided SWIPT system. Our key contributions are outlined as

follows:

- We develop an RIS-assisted ISAC architecture that enables efficient SWIPT, improving both communication and sensing performance.
- In this paper, we propose a dual function base station (DFBS) capable of simultaneously transmitting signals to both targets and communication users. To enhance precise target detection in the radar application, we incorporate A-RIS technology. Additionally, the system supports communication and energy harvesting through the use of STAR-RIS for SWIPT system.
- We formulate and solve a joint optimization problem to minimize the target constraint while maximizing the communication rate which implies the trade-offs between target sensing accuracy and communication performance, demonstrating the potential of RISs to enhance system capabilities in diverse ISAC scenarios.
- To solve the challenging sum-rate maximization problem in an ISAC system we adopt the minimum mean square error (MMSE), which transform the original problem into its equivalent sub problems. Later we optimize transmit beamforming and phase-shift beamforming independently in a iterative manner using general approximations like standard package solver CVX, successive convex approximation (SCA), and majorization minimization (MM) methods.
- Additionally, we investigate the impact of imperfect channel state information (CSI) on the performance of the ISAC-enabled SWIPT and full-duplex amplify-forward relay over STAR-RIS. The numerical results are provided to evaluate the interpretation of the proposed STAR-RIS-assisted SWIPT system in comparison with the traditional passive RIS-based SWIPT system under different network parameters, including the density and location of reflecting and transmitting energy devices (R-EDs, T-EDs) and communication users (R-CUs, T-CUs), the number of STAR-RIS elements, the sensing threshold, and other factors.
- Specifically, detailed numerical analysis reveals that the STAR-RIS architecture can significantly enhance the beamforming gain by 12-15% compared to the traditional passive RIS, while still meeting the required QoS constraints for ISAC-assisted SWIPT systems. On the other hand, the traditional RIS system requires higher transmission power and more passive elements (i.e., higher resource consumption) as compared to STAR-RIS to achieve the same QoS, demonstrating the superior efficiency and performance benefits of the STAR-RIS design.

Organization of the paper: The paper is summarized as follows. Section II, and Section III state the system model and problem formulation, respectively. Section IV describes the proposed solution, and Section V presents the simulation results to show the superiority of the proposed scheme. Finally, Section VI concludes this paper.

Notations: Throughout this paper, we use $\mathbf{A}$ for matrix, $\mathbf{a}$ for vector, a for scalar, $|\mathbf{A}|$ means determinant, $\mathbf{a}^T$ for transpose of $\mathbf{a}$, $\mathbf{a}^H$ for Hermitian (conjugate transpose) of $\mathbf{a}$, a^{-1} for inverse, $\mathcal{R}(a)$ is for real part of a, $\mathbb{C}^{M\times M}$ for complex matrix, $\mathbb{C}^{M\times 1}$ for complex vector, $||\mathbf{a}||$ represents norm of a vector and diag(a) for diagonalization operator. $||\cdot||_F$ denotes the Fibonacci's norm.

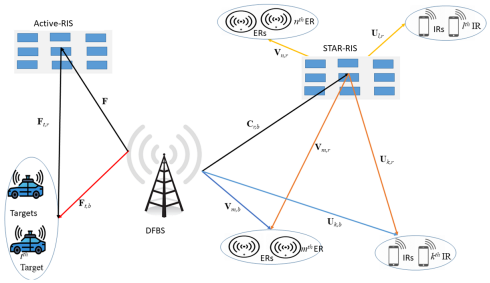

Fig. 1: RIS-assisted MIMO ISAC model with SWIPT.

II. System Model

Let us consider a DFBS equipped with N_B transmit/receive antennas, transmitting signals to a set of reflection energy devices (R-EDs) denoted as $\mathcal{M} = \{1, \ldots, M\}$, each equipped with N_{E_r} antennas. Additionally, there is a set of transmission energy devices (T-EDs) denoted as $\mathcal{N} = \{1, \ldots, N\}$, each with N_{E_t} antennas. We also have a collection of reflection communication users (R-CUs) represented by set $\mathcal{K} = \{1, \ldots, K\}$, where each user possesses N_{I_r} antennas, and a set of transmission communication users (T-CUs) denoted as $\mathcal{L} = \{1, \ldots, L\}$, with N_{I_t} antennas. Furthermore, we have a set of sensing targets (STs) labeled as $\mathcal{T} = \{1, \ldots, T\}$, each equipped with N_T antennas. The STAR-RIS (STAR-RIS) are equipped with $\mathcal{Z} = \{1, \ldots, Z\}$ number of reflection/transmission elements serving communication users and the active-RIS is equipped with $\mathcal{N}_{R_a} = \{1, \ldots, N_{R_a}\}$ number of reflection elements with active loads serving radar targets. In our study, we consider a scenario where the direct signal path is affected by non-line-of-sight (NLoS) conditions for the long distance receivers. In such situations, RISs take on a fascinating role by effectively acting as signal sources for the receivers. Consequently, each receiver's objective is to receive signals from both the direct path and the RIS-assisted path. **STAR-RIS for Communication in Energy Splitting Mode:** In order to address the limitations associated with conventional RISs, which are typically constrained to providing communication coverage over half of the space $(180°)$, we have incorporated the concept of STAR-RIS into our SWIPT system. This innovation extends communication coverage to a full $360°$.

Let s_z represents the incident signal on the z^{th} element of the STAR-RIS, where $z\{r,t\} \in \mathcal{Z} \triangleq \{1, 2, \ldots, Z\}$ and Z denotes the quantity of STAR-RIS elements. Therefore, the transmitted and reflected (TAR) signals by the z^{th} element can be represented by utilizing transmission and reflection coefficients as [44] $\phi_{r_z} = \left(\sqrt{\beta_z^r} e^{j\theta_z^r}\right) s_z$ and $\phi_{t_z} = \left(\sqrt{\beta_z^t} e^{j\theta_z^t}\right) s_z$, where $\sqrt{\beta_z^r}, \sqrt{\beta_z^t} \in [0, 1]$ are the magnitude coefficient and $\theta_z^r, \theta_z^t \in [0, 2\pi)$ are the phase-shift for the respective reflection and transmission coefficient of the z^{th} STAR-RIS element.

Overall, the TAR coefficient matrices of STAR-RIS can be expressed as

$$\mathbf{\Phi}_r = \text{diag}(\sqrt{\beta_1^r}e^{j\theta_1^r}, \sqrt{\beta_2^r}e^{j\theta_2^r}, \cdots, \sqrt{\beta_Z^r}e^{j\theta_Z^r}), \quad (1)$$

$$\mathbf{\Phi}_t = \text{diag}(\sqrt{\beta_1^t}e^{j\theta_1^t}, \sqrt{\beta_2^t}e^{j\theta_2^t}, \cdots, \sqrt{\beta_Z^t}e^{j\theta_Z^t}), \quad (2)$$

Note that, we assume the reflection and transmission coefficients (RTCs), specifically θ_z^r and θ_z^t, for each element can generally be chosen independently [44]. However, the variations in magnitude for RTCs (i.e., $\sqrt{\beta_z^r}$ and $\sqrt{\beta_z^t}$) are interconnected with the principle of energy conservation. In other words, for each element of RIS, the combined energies of the TAR signals [1], lossless STAR-RIS is equal to the incident signal's energy. Mathematically, this is expressed as $|r_z|^2 + |t_z|^2 = |s_z|^2$ that provides the condition for TAR intensity factor of every STAR-RIS component [45]:

$$\beta_z^t + \beta_z^r = 1, \forall z \in \mathcal{Z}. \quad (3)$$

A-RIS for Sensing: In order to enhance the radar system's ability to achieve a finer angular resolution in received signals, it necessitates an increase in power. Consequently, for the purpose of precise target detection in our radar application, we have chosen to incorporate active RIS technology. This active RIS can amplify the signals with additional power, improving overall detection accuracy. Therefore, the reflection matrix at the A-RIS is defined as in [46]:

$$\mathbf{\Theta} = \text{diag}[\phi_1, \phi_2, \ldots, \phi_{N_{R_a}}] \in \mathbb{C}^{N_{R_a} \times N_{R_a}}, \quad (4)$$

where $\phi \triangleq \kappa_j e^{j\theta}$ is the reflection coefficient of the n-th element of the ARIS[2]. It should be noted that the amplification factor in an A-RIS functions as a power source for each element, amplifying the incident signals directed toward the A-RIS. This amplification boosts the channel gain towards the targets.

A. Downlink Signal Model

The BS designs the combined precoder for all the users, which is given by

$$\mathbf{x} = \sum_{k=1}^{K} \mathbf{W}_k \mathbf{s}_k + \sum_{l=1}^{L} \mathbf{W}_l \mathbf{s}_l + \sum_{t=1}^{T} \mathbf{W}_t \mathbf{s}_t, \quad (5)$$

where $\mathbf{W}_k \in^{N_B \times D_s}, \mathbf{W}_l \in^{N_B \times D_s}$ and $\mathbf{W}_t \in^{N_B \times D_s}$ are the precoders designed at the DFBS for k^{th} R-CUs, l^{th} T-CUs and t^{th} STs, respectively and $\mathbf{s}_k \in^{D_S \times 1}, \mathbf{s}_l \in^{D_S \times 1}$ and $\mathbf{s}_t \in^{D_S \times 1}$ are the number of data streams transmitted via respective precoders while satisfying $\mathbb{E}[\mathbf{s}_k \mathbf{s}_k^{\text{H}}] = \mathbb{E}[\mathbf{s}_l \mathbf{s}_l^{\text{H}}] = \mathbb{E}[\mathbf{s}_t \mathbf{s}_t^{\text{H}}] \triangleq \mathbf{I}_{D_s}$ and $\mathbb{E}[\mathbf{s}_k \mathbf{s}_{k'}^{\text{H}}] = \mathbb{E}[\mathbf{s}_l \mathbf{s}_{l'}^{\text{H}}] = \mathbb{E}[\mathbf{s}_t \mathbf{s}_{t'}^{\text{H}}] \triangleq \mathbf{0}, k \neq k', l \neq l'$ and $t \neq t'$.

Remark 1. *The total power required to transmit the signals from DFBS is designed using the following expression.*

$$\mathbf{W} \triangleq P_b = \sum_{k=1}^{K} \|\mathbf{W}_k\|_F^2 + \sum_{l=1}^{L} \|\mathbf{W}_l\|_F^2 + \sum_{t=1}^{T} \|\mathbf{W}_t\|_F^2. \quad (6)$$

The DFBS power is strictly limited by the total available power available at the source, which is defined as $P_b \leq P_{max}^{DFBS}$.

B. MIMO SWIPT Metric

In the following subsections, we aim to obtain and optimize the communication throughput and energy efficiency simultaneously using STAR-RIS, while considering the radar targets as an interference.

C. Information Transfer Model:

We assume that all the channels are perfectly known by the DFBS[3]. By denoting the transmit signal at DFBS, the received signals at the k^{th} R-IR and the l^{th} T-IR are given by

$$\mathbf{y}_k = (\mathbf{U}_{k,b} + \mathbf{U}_{k,r} \mathbf{\Phi} \mathbf{C}_{r,b}) \mathbf{x} + \mathbf{n}_k \quad (7)$$

$$\mathbf{y}_l = (\mathbf{U}_{l,r} \mathbf{\Phi} \mathbf{C}_{r,b}) \mathbf{x} + \mathbf{n}_l \quad (8)$$

where $\mathbf{U}_{k,b} \in^{N_{I_r} \times N_B}$, $\mathbf{U}_{k,r} \in^{N_{I_r} \times Z}$, $\mathbf{C}_{r,b} \in^{Z \times N_B}$, $\mathbf{U}_{l,r} \in^{N_{I_t} \times Z}$, represents the channel between DFBS-k^{th}R-CUs, STAR-RIS-k^{th}R-CUs, DFBS-STAR-RIS, and STAR-RIS-l^{th}T-CUs, respectively and $\mathbf{n}_k \sim \mathcal{CN}(0, \sigma_k^2 \mathbf{I}_{N_{I_r}})$ and $\mathbf{n}_l \sim \mathcal{CN}(0, \sigma_l^2 \mathbf{I}_{N_{I_t}})$ represents the additive white Gaussian noise (AWGN) of R-CUs and T-CUs with zero-mean and σ_k^2 and σ_l^2 variance, respectively.

Inserting (5) into (7) and (8), the received signals at the k^{th} R-CU and the l^{th} T-CU are transformed as (9) and (10), respectively, shown on the top of the next page, where $\bar{\mathbf{U}}_k = \mathbf{U}_{k,b} + \mathbf{U}_{k,r} \mathbf{\Phi} \mathbf{C}_{r,b}$ and $\bar{\mathbf{U}}_l = \mathbf{U}_{l,r} \mathbf{\Phi} \mathbf{C}_{r,b}$ represent equivalent channels at k^{th} R-CU and l^{th} T-CU, respectively.

By obtaining the received signals, the rate expressions at the k^{th} R-CU and the l^{th} T-CU are modelled as

$$R_k(\mathbf{W}_k, \mathbf{\Phi}) = \log_2 |\mathbf{I} + \bar{\mathbf{U}}_k \mathbf{W}_k \mathbf{W}_k^{\text{H}} \bar{\mathbf{U}}_k^{\text{H}} \mathbf{J}_k^{-1}| \quad (11)$$

$$R_l(\mathbf{W}_l, \mathbf{\Phi}) = \log_2 |\mathbf{I} + \bar{\mathbf{U}}_l \mathbf{W}_l \mathbf{W}_l^{\text{H}} \bar{\mathbf{U}}_l^{\text{H}} \mathbf{J}_l^{-1}| \quad (12)$$

where $\mathbf{J}_k = \sum_{i \neq k}^{K} \bar{\mathbf{U}}_k \mathbf{W}_i \mathbf{W}_i^{\text{H}} \bar{\mathbf{U}}_k^{\text{H}} + \sum_{l=1}^{L} \bar{\mathbf{U}}_k \mathbf{W}_l \mathbf{W}_l^{\text{H}} \mathbf{U}_k^{\text{H}} + \sum_{t=1}^{T} \bar{\mathbf{U}}_k \mathbf{W}_t \mathbf{W}_t^{\text{H}} \bar{\mathbf{U}}_k^{\text{H}} + \sigma_k^2$ and $\mathbf{J}_l = \sum_{i \neq l}^{L} \bar{\mathbf{U}}_l \mathbf{W}_i \mathbf{W}_i^{\text{H}} \bar{\mathbf{U}}_l^{\text{H}} + \sum_{k=1}^{K} \bar{\mathbf{U}}_l \mathbf{W}_k \mathbf{W}_k^{\text{H}} \mathbf{U}_l^{\text{H}} + \sum_{t=1}^{T} \bar{\mathbf{U}}_l \mathbf{W}_t \mathbf{W}_t^{\text{H}} \bar{\mathbf{U}}_l^{\text{H}} + \sigma_l^2$ are defined as interference plus noise ratio at k^{th} R-CU and l^{th} T-CU, respectively.

D. Power Transfer Model:

It's worth mentioning that electromagnetic waves naturally transmitted through wireless channels can serve as a source of power for EDs. In this context, we opted for straightforward linear energy harvesting (EH) for simplicity, as in [47].

Remark 2. *The amount of harvested power is contingent on the input RF power level and is typically non-linear concerning the received RF power. To be precise, the adoption of the linear EH model represents an approximation due to the*

[1]In this paper, we examine a lossless STAR-RIS surface that does not experience any power loss during the reflection and transmission (RAT) of the signal. Nonetheless, the analysis presented can also be applied to a lossy surface where $\beta_z^r + \beta_z^t < 1 \ \forall z$.

[2]If the amplification factor falls within the range $0 \leq \kappa_j \leq 1$, the A-RIS in our study behaves as a Passive RIS.

[3]DFBS can accurately determine the channel using pilot symbols. However, obtaining the optimal value for the adopted problem is challenging, leading us to assume perfect channel state information (CSI). Nevertheless, it's important to note that the problem readily extends to scenarios with imperfect CSI.

$$\mathbf{y}_k = \underbrace{\bar{\mathbf{U}}_k \mathbf{W}_k \mathbf{s}_k}_{\text{Desired R-IR signal}} + \underbrace{\bar{\mathbf{U}}_k \sum\nolimits_{i\neq k}^{K} \mathbf{W}_i \mathbf{s}_i}_{\text{IUI}} + \underbrace{\bar{\mathbf{U}}_k \sum\nolimits_{l=1}^{L} \mathbf{W}_l \mathbf{s}_l}_{\text{T-IRs Interefence}} + \underbrace{\bar{\mathbf{U}}_k \sum\nolimits_{t=1}^{T} \mathbf{W}_t \mathbf{s}_t + \mathbf{n}_k}_{\text{Target Interefence plus AWGN}} \tag{9}$$

$$\mathbf{y}_l = \underbrace{\bar{\mathbf{U}}_l \mathbf{W}_l \mathbf{s}_l}_{\text{Desired T-IR signal}} + \underbrace{\bar{\mathbf{U}}_l \sum\nolimits_{i\neq l}^{L} \mathbf{W}_i \mathbf{s}_i}_{\text{IUI}} + \underbrace{\bar{\mathbf{U}}_l \sum\nolimits_{k=1}^{K} \mathbf{W}_k \mathbf{s}_k}_{\text{R-IRs Interefence}} + \underbrace{\bar{\mathbf{U}}_l \sum\nolimits_{t=1}^{T} \mathbf{W}_t \mathbf{s}_t + \mathbf{n}_l}_{\text{Target Interefence plus AWGN}} \tag{10}$$

inherent non-linear characteristics of both active and passive components involved in energy harvesting, as elaborated in the work by [48]. While employing a non-linear EH model may offer a more realistic depiction of the dual RIS-assisted SWIPT system, it introduces complexity to the beamforming design and resource allocation problem. Furthermore, it deviates from the central objective of this manuscript, which is to examine the enhancements in performance realized through the SWIPT-enabled RIS framework incorporating ISAC. As a result, we have chosen to work with a linear energy harvesting model in this study, with plans to delve into an analysis with the non-linear energy harvesting model in future research.

Therefore, the received signals at the m^{th} R-ED and the n^{th} T-ED are given respectively by

$$\mathbf{y}_m = (\mathbf{V}_{m,b} + \mathbf{V}_{m,r}\mathbf{\Phi}\mathbf{C}_{r,b})\mathbf{x} + \mathbf{n}_m, \tag{13}$$

$$\mathbf{y}_n = (\mathbf{V}_{n,r}\mathbf{\Phi}\mathbf{C}_{r,b})\mathbf{x} + \mathbf{n}_n, \tag{14}$$

where $\mathbf{V}_{m,b} \in^{N_{E_r}\times N_B}$, $\mathbf{V}_{m,r} \in^{N_{E_r}\times Z}$, and $\mathbf{V}_{n,r} \in^{N_{E_t}\times Z}$, represent the channel matrices from DFBS- m^{th}R-EDs, m^{th} R-EDs-STAR-RIS, and STAR-RIS- n^{th}T-EDs, respectively. Upon inserting the (5) into (13), (14) and neglecting the interference plus noise ratio, the received signal is directly proportional to the power, which is given by

$$V_m = \eta \,\mathrm{Tr}\left(\sum\nolimits_{k=1}^{K} \bar{\mathbf{V}}_m \mathbf{W}_k \mathbf{W}_k^{\mathrm{H}} \bar{\mathbf{V}}_m^{\mathrm{H}}\right), \tag{15}$$

$$V_n = \iota \,\mathrm{Tr}\left(\sum\nolimits_{l=1}^{L} \bar{\mathbf{V}}_n \mathbf{W}_l \mathbf{W}_l^{\mathrm{H}} \bar{\mathbf{V}}_n^{\mathrm{H}}\right), \tag{16}$$

where $\bar{\mathbf{V}}_m \triangleq \mathbf{V}_{m,b} + \mathbf{V}_{m,r}\mathbf{\Phi}\mathbf{C}_{r,b}$ and $\bar{\mathbf{V}}_n \triangleq \mathbf{V}_{n,r}\mathbf{\Phi}\mathbf{C}_{r,b}$, represent the equivalents channels for R-EDs and T-EDs, respectively. η and ι are defined as energy efficiency factor for all R-EDs and T-EDs, respectively. By introducing α_r as a weighting factor for R-EDs and α_t as weighting factor at T-EDs, the expressions in (15) and (16) are rewritten as

$$V_{tot} \triangleq V_{totm}^{pow} = \mathrm{Tr}\left(\sum\nolimits_{k=1}^{K} \mathbf{W}_k^{\mathrm{H}} \mathbf{V}_{tm} \mathbf{W}_k\right), \tag{17}$$

$$Q_{tot} \triangleq V_{totn}^{pow} = \mathrm{Tr}\left(\sum\nolimits_{l=1}^{L} \mathbf{W}_l^{\mathrm{H}} \mathbf{V}_{tn} \mathbf{W}_l\right), \tag{18}$$

where $\mathbf{V}_{tm} = \eta\alpha_r \sum_{m=1}^{M} \bar{\mathbf{V}}_m^{\mathrm{H}} \bar{\mathbf{V}}_m$ and $\mathbf{V}_{tn} = \iota\alpha_t \sum_{n=1}^{N} \bar{\mathbf{V}}_n^{\mathrm{H}} \bar{\mathbf{V}}_n$.

Remark 3. *By obtaining the rate expressions at the communication metric the total achievable rate (bits/s/Hz) of the desired communication system is given by*

$$R_c = \sum\nolimits_{k=1}^{K} R_k + \sum\nolimits_{l=1}^{L} R_l, \tag{19}$$

where R_c represents the total sum rate for both R-CUs and T-CUs.

E. Sensing Metric

From the standpoint of radar detection, because the probability of detecting a target is directly linked to the radar's signal-to-interference-noise ratio (SINR), our objective is to analysis the impact of the sensing constraints on the communication system, minimizing the sensing interference on the SWIPT system and by taking into account an A-RIS, to enhance the sensing performance. As shown in Fig.1, the transmitted probing signal reaches the t^{th} target via both the direct path (indicated by the red solid line) and the reflected path (illustrated by the black solid line), before returning to the DFBS through all the propagation links. It is important to mention that any propagation delay between these paths is minimal and is not considered in our analysis. Consequently, the combined echo signal collected from the DFBS from the t^{th} target can be expressed as [49]

$$\mathbf{y}_t = \mathbf{F}_{r,b}\mathbf{x} + [\mathbf{F}_{t,r}\mathbf{\Theta}(\mathbf{F}\mathbf{x} + \mathbf{z}_0)] + \mathbf{n}_b, \tag{20}$$

where $\mathbf{F}_{t,b} \in^{N_T\times N_B}$, $\mathbf{F}_{t,r} \in^{N_T\times N_{R_a}}$, and $\mathbf{F}_{r,b} \in^{N_{R_a}\times N_B}$ are the channels from DFBS-t^{th}STs, A-RIS-t^{th}STs, and DFBS-A-RIS, respectively and $\mathbf{n}_t \sim \mathcal{CN}(0, \sigma_t^2 \mathbf{I}_{N_T})$ denotes the AWGN.

Inserting (5) into (20), we get

$$\mathbf{y}_t = \underbrace{\bar{\mathbf{F}}_t \mathbf{W}_t \mathbf{s}_t}_{\text{Desired Target signal}} + \underbrace{\bar{\mathbf{F}}_t \sum\nolimits_{i\neq t}^{T} \mathbf{W}_i \mathbf{s}_i}_{\text{IUI}} + \underbrace{\bar{\mathbf{F}}_t \sum\nolimits_{k=1}^{K} \mathbf{W}_k \mathbf{s}_k}_{\text{R-IRs Interefence}} + \underbrace{\bar{\mathbf{F}}_t \sum\nolimits_{l=1}^{L} \mathbf{W}_l \mathbf{s}_l + \mathbf{F}_{t,r}\mathbf{\Theta}\mathbf{z}_0 + \mathbf{n}_t}_{\text{T-IRs Interefence plus A-RIS noise plus AWGN}}, \tag{21}$$

where $\bar{\mathbf{F}}_t = \mathbf{F}_{t,b} + \mathbf{F}_{t,r}\mathbf{\Theta}\mathbf{F}_{r,b}$ is equivalent channel at the t^{th} target. Thus, the rate expression at the t^{th} target is obtained as

$$R_t(\mathbf{W}_t, \mathbf{\Theta}) = \log_2|\mathbf{I} + \bar{\mathbf{F}}_t \mathbf{W}_t \mathbf{W}_t^{\mathrm{H}} \bar{\mathbf{F}}_t^{\mathrm{H}} \mathbf{J}_t^{-1}|, \tag{22}$$

where $\mathbf{J}_t = \sum_{i\neq t}^{T} \bar{\mathbf{F}}_t \mathbf{W}_i \mathbf{W}_i^{\mathrm{H}} \bar{\mathbf{F}}_t^{\mathrm{H}} + \sum_{k=1}^{K} \bar{\mathbf{F}}_t \mathbf{W}_k \mathbf{W}_k^{\mathrm{H}} \mathbf{F}_t^{\mathrm{H}} + \sum_{l=1}^{K_t} \bar{\mathbf{F}}_t \mathbf{W}_l \mathbf{W}_l^{\mathrm{H}} \bar{\mathbf{F}}_t^{\mathrm{H}} + \sigma_g^2 \mathbf{F}_{t,r}\mathbf{\Theta}\mathbf{\Theta}^{\mathrm{H}}\mathbf{F}_{t,r}^{\mathrm{H}} + \sigma_t^2$ is interference plus noise ratio at t^{th} target.

Remark 4. *The total power consumed at the A-RIS elements due to its amplification to detect the radar targets is given by*

$$P_{ARIS} = P_s + P_d, \tag{23}$$

where P_s and P_d are representative of the static and dynamic power usage elements in an A-RIS system. Specifically, these components encapsulate the power expended by various constituents of the A-RIS. This power consumption encompasses both the static power and direct current (DC) biasing power, in addition to the power utilized by the hardware unit, as

specified in [46]. The dynamic power of an amplifier pertains to the energy it consumes when transmitting a signal from the ARIS, and this can be expressed as [46]

$$P_d = \alpha \sum_{t=1}^{T} \|(\boldsymbol{\Theta}\mathbf{F}_{r,b}\mathbf{W}_t)\|^2 + \sigma_g^2 \|\boldsymbol{\Theta}\|_F^2, \tag{24}$$

where α is the amplifier efficiency of A-RIS element. The static power at the A-RIS is defined as

$$P_s = N_{R_a} W_1 + N_2 W_2, \tag{25}$$

where W_1 and W_2 represents the noise figure of A-RIS, corresponding to the phase-shift circuit and power amplifier, respectively. N_2 represents the number of required power amplifiers.

III. Problem Formulation

The main objective of this work is to maximize the sum-rate at R-CUs and T-CUs, while satisfying the sensing constraint by jointly optimizing the precoder matrix $\mathbf{W}$ at the DFBS, the phase shift matrix $\boldsymbol{\Phi}$ at the STAR-RIS, and the reflection phase-shift matrix $\boldsymbol{\Theta}$ at A-RIS is expressed as

$$\begin{aligned}
(\mathcal{P}_1): \quad & \max_{\mathbf{W},\boldsymbol{\Phi},\boldsymbol{\Theta}} && R_c && \text{(26a)}\\
& \text{s.t.} && P_b \le P_{max}^{DFBS} && \text{(26b)}\\
& && V_{tot} \ge \bar{V}_{min}^{\text{pow}}, && \text{(26c)}\\
& && Q_{tot} \ge \bar{Q}_{min}^{\text{pow}}, && \text{(26d)}\\
& && \theta_z^t, \theta_z^r \in [0, 2\pi), \ \forall z \in \mathcal{Z}, && \text{(26e)}\\
& && \beta_z^r + \beta_z^t = 1, \ \ 0 \le \beta_z^r, \beta_z^t \le 1, \ \ \forall z \in \mathcal{Z}, && \text{(26f)}\\
& && R_t \ge R_{\min}^{sens}, && \text{(26g)}\\
& && a_r \le a_{max} \forall r \in \mathcal{N}_{R_a}, && \text{(26h)}\\
& && P_{ARIS} \le P_{max}^{A-RIS}, && \text{(26i)}
\end{aligned}$$

However, the objective function $\mathcal{P}_1$ in (26) is NP-hard problem, due to strong coupling of variables, i.e., transmit beamforming matrices and STAR-RIS phase shift beamforming matrices in (26a). Therefore, it is hard to derive the closed-form expression for the formulated problem. Therefore, we opt the alternate optimization method to transform it into equivalent sub-problems and solve in a iterative manner. The R-EH and, T-RH constraints are defined in (26c), and (26d) which are also non-convex in nature. Therefore, first we convert the non-convex constraint into convex form. (26g) is the sensing constraint, which acts as an interference to the communication system. Furthermore, the (26e), (26f), (26h), and (26i), are the STAR-RIS and A-RIS constraints, respectively. In the following sections, we present the study of low-complexity algorithm to solve the formulated problem.

IV. Proposed Solution

In this section, we break down problem (26) into two more manageable sub-problems and create efficient algorithms to iteratively address them.

A. MMSE Trasnformation

The formulated problem (26), is jointly non-convex. To solve this problem, we adopt the well-known minimum mean square error (MMSE) method [19]. Therefore, the estimated signal vector of the received signal at k^{th} R-CU and l^{th} T-CU are given by

$$\hat{\mathbf{e}}_k = \mathbf{D}_k^{\mathrm{H}} y_k, \quad \hat{\mathbf{e}}_l = \mathbf{D}_l^{\mathrm{H}} y_l, \tag{27}$$

where $\mathbf{D}_k \in \mathbb{C}^{N_{I_r} \times D_s}$ and $\mathbf{D}_l \in \mathbb{C}^{N_{E_r} \times D_s}$ denotes the linear decoding matrix of the estimated signal. The MSE of the estimated signal at k^{th} R-CU is given by

$$\begin{aligned}
\mathbf{E}_k =& \mathbb{E}\left[(\hat{\mathbf{e}}_k - \mathbf{e}_k)(\hat{\mathbf{e}}_k - \mathbf{e}_k)^{\mathrm{H}}\right]\\
=& \left(\mathbf{D}_k^{\mathrm{H}}\bar{\mathbf{U}}_k\mathbf{W}_k - \mathbf{I}_{D_s}\right)\left(\mathbf{D}_k^{\mathrm{H}}\bar{\mathbf{U}}_k\mathbf{W}_k - \mathbf{I}_{D_s}\right)^{\mathrm{H}}\\
&+ \sum_{i\neq k}^{\mathcal{K}} \mathbf{D}_k^{\mathrm{H}}\bar{\mathbf{U}}_k\mathbf{W}_i\mathbf{W}_i^{\mathrm{H}}\bar{\mathbf{U}}_k^{\mathrm{H}}\mathbf{D}_k + \sigma_I^2\mathbf{D}_k^{\mathrm{H}}\mathbf{D}_k\\
&+ \sum_{l=1}^{\mathcal{L}} \mathbf{D}_k^{\mathrm{H}}\bar{\mathbf{U}}_k\mathbf{W}_l\mathbf{W}_l^{\mathrm{H}}\bar{\mathbf{U}}_k^{\mathrm{H}}\mathbf{D}_k\\
&+ \sum_{t=1}^{\mathcal{T}} \mathbf{D}_k^{\mathrm{H}}\bar{\mathbf{U}}_k\mathbf{W}_t\mathbf{W}_t^{\mathrm{H}}\bar{\mathbf{U}}_k^{\mathrm{H}}\mathbf{D}_k.
\end{aligned} \tag{28}$$

Similarly, the MSE of the estimated signal at the l^{th} T-CU is given by

$$\begin{aligned}
\mathbf{E}_l =& \mathbb{E}\left[(\hat{\mathbf{e}}_l - \mathbf{e}_l)(\hat{\mathbf{e}}_l - \mathbf{e}_l)^{\mathrm{H}}\right]\\
=& \left(\mathbf{D}_l^{\mathrm{H}}\bar{\mathbf{U}}_l\mathbf{W}_l - \mathbf{I}_{D_s}\right)\left(\mathbf{D}_l^{\mathrm{H}}\bar{\mathbf{U}}_l\mathbf{W}_l - \mathbf{I}_{D_s}\right)^{\mathrm{H}}\\
&+ \sum_{i\neq l}^{\mathcal{L}} \mathbf{D}_l^{\mathrm{H}}\bar{\mathbf{U}}_l\mathbf{W}_i\mathbf{W}_i^{\mathrm{H}}\bar{\mathbf{U}}_l^{\mathrm{H}}\mathbf{D}_l + \sigma_I^2\mathbf{D}_l^{\mathrm{H}}\mathbf{D}_l\\
&+ \sum_{k=1}^{\mathcal{K}} \mathbf{D}_l^{\mathrm{H}}\bar{\mathbf{U}}_l\mathbf{W}_k\mathbf{W}_k^{\mathrm{H}}\bar{\mathbf{U}}_l^{\mathrm{H}}\mathbf{D}_l\\
&+ \sum_{t=1}^{\mathcal{T}} \mathbf{D}_l^{\mathrm{H}}\bar{\mathbf{U}}_l\mathbf{W}_t\mathbf{W}_t^{\mathrm{H}}\bar{\mathbf{U}}_l^{\mathrm{H}}\mathbf{D}_{kl}.
\end{aligned} \tag{29}$$

By denoting the auxiliary matrix $\mathbf{A}$, the problem in (26) is transformed as follows:

$$(\mathcal{P}_2): \min_{\mathbf{W},\boldsymbol{\Phi},\mathbf{D},\mathbf{A}} \quad \widehat{R}_c \qquad \text{s.t.} \quad \text{(26b)} - \text{(26i)}, \tag{30}$$

where $\widehat{R}_c(\mathbf{W},\boldsymbol{\Phi},\mathbf{D},\mathbf{A}) = \left\{\log|\mathbf{A}_k| - \mathrm{Tr}\left(\mathbf{A}_k\mathbf{E}_k\right) + D_s\right\} + \left\{\log|\mathbf{A}_l| - \mathrm{Tr}\left(\mathbf{A}_l\mathbf{E}_l\right) + D_s\right\}$ Note the problem (30) is still jointly non-convex and more complex to solve compared to problem (26), due to highly couple of variables. Therefore, we optimize each variable separately in a iterative way until it reach the optimal value. Therefore, by doing partial derivative of $\widehat{R}_k$ w.r.t $\mathbf{D}_k$ and $\mathbf{A}_k$ to zero, is given by

$$\mathbf{D}_k^{\star} = \left(\mathbf{J}_k + \bar{\mathbf{U}}_k\mathbf{W}_k\mathbf{W}_k^{\mathrm{H}}\bar{\mathbf{U}}_k^{\mathrm{H}}\right)^{-1}\bar{\mathbf{U}}_k\mathbf{W}_k, \tag{31}$$

$$\mathbf{A}_k^{\star} = \mathbf{E}_k^{\star -1}. \tag{32}$$

Liskewise, by doing partial derivative of $\widehat{R}_l$ w.r.t $\mathbf{D}_l$ and $\mathbf{A}_l$ to zero, is given by

$$\mathbf{D}_l^{\star} = \left(\mathbf{J}_l + \bar{\mathbf{U}}_l\mathbf{W}_l\mathbf{W}_l^{\mathrm{H}}\bar{\mathbf{U}}_l^{\mathrm{H}}\right)^{-1}\bar{\mathbf{U}}_l\mathbf{W}_l, \tag{33}$$

$$\mathbf{A}_l^{\star} = \mathbf{E}_l^{\star -1}. \tag{34}$$

By inserting (31) into (28), the optimal $\mathbf{E}_k^{\star}$ is obtained as in (35) and substituting (33) into (29), the optimal $\mathbf{E}_l^{\star}$ is obtained as in (36) as shown on the top of the next page. In the following sections, we aim to optimize the transmit beamforming matrix $\mathbf{W}$ at DFBS and phase-shift matrix $\boldsymbol{\Phi}$ of the STAR-RIS, while suppressing the radar interference.

$$\mathbf{E}_k^\star = \mathbf{I}_{D_s} - \mathbf{W}_k^{\mathrm{H}}\bar{\mathbf{U}}_k^{\mathrm{H}}\left(\sum_{i\in\mathcal{K}}\bar{\mathbf{U}}_k\mathbf{W}_i\mathbf{W}_i^{\mathrm{H}}\bar{\mathbf{U}}_k^{\mathrm{H}} + \sigma_I^2\mathbf{I} + \sum_{l\in\mathcal{L}}\bar{\mathbf{U}}_k\mathbf{W}_l\mathbf{W}_l^{\mathrm{H}}\bar{\mathbf{U}}_k^{\mathrm{H}} + \sum_{t\in\mathcal{T}}\bar{\mathbf{U}}_k\mathbf{W}_t\mathbf{W}_t^{\mathrm{H}}\bar{\mathbf{U}}_k^{\mathrm{H}}\right)^{-1}\bar{\mathbf{U}}_k\mathbf{W}_k. \quad (35)$$

$$\mathbf{E}_l^\star = \mathbf{I}_{D_s} - \mathbf{W}_l^{\mathrm{H}}\bar{\mathbf{U}}_l^{\mathrm{H}}\left(\sum_{i\in\mathcal{L}}\bar{\mathbf{U}}_l\mathbf{W}_i\mathbf{W}_i^{\mathrm{H}}\bar{\mathbf{U}}_l^{\mathrm{H}} + \sigma_I^2\mathbf{I} + \sum_{k\in\mathcal{K}}\bar{\mathbf{U}}_l\mathbf{W}_k\mathbf{W}_k^{\mathrm{H}}\bar{\mathbf{U}}_l^{\mathrm{H}} + \sum_{t\in\mathcal{T}}\bar{\mathbf{U}}_l\mathbf{W}_t\mathbf{W}_t^{\mathrm{H}}\bar{\mathbf{U}}_l^{\mathrm{H}}\right)^{-1}\bar{\mathbf{U}}_l\mathbf{W}_l. \quad (36)$$

B. Optimize $\mathbf{W}$ *for given* $\mathbf{\Phi}$

In this section, for the obtained optimal $\mathbf{D}, \mathbf{A}, \mathbf{E}$, and given $\mathbf{\Phi}$, we aim to optimize the $\mathbf{W}$. Therefore by inserting MSE in (28), and (29) into problem (30) and excluding the terms independent of $\mathbf{W}$, $(\mathcal{P}_2)$ is given by

$$\begin{aligned}(\mathcal{P}_{2a}): \min_{\mathbf{W}} \;& \sum_{k=1}^{K}\mathrm{tr}\left(\mathbf{W}_k^{\mathrm{H}}\mathbf{B}_k\mathbf{W}_k\right) - \sum_{k=1}^{K}\mathrm{tr}\left(\mathbf{A}_k\mathbf{D}_k^{\mathrm{H}}\bar{\mathbf{U}}_k\mathbf{W}_k\right) \\ & - \sum_{k=1}^{K}\mathrm{tr}\left(\mathbf{A}_k\mathbf{W}_k^{\mathrm{H}}\bar{\mathbf{U}}_k^{\mathrm{H}}\mathbf{D}_k\right) + \sum_{l=1}^{L}\mathrm{tr}\left(\mathbf{W}_l^{\mathrm{H}}\mathbf{B}_k\mathbf{W}_l\right) \\ & + \sum_{t=1}^{T}\mathrm{tr}\left(\mathbf{W}_t^{\mathrm{H}}\mathbf{B}_k\mathbf{W}_t\right) + \sum_{l=1}^{L}\mathrm{tr}\left(\mathbf{W}_l^{\mathrm{H}}\mathbf{B}_l\mathbf{W}_l\right) \\ & - \sum_{l=1}^{L}\mathrm{tr}\left(\mathbf{A}_l\mathbf{D}_l^{\mathrm{H}}\bar{\mathbf{U}}_l\mathbf{W}_l\right) - \sum_{l=1}^{L}\mathrm{tr}\left(\mathbf{A}_l\mathbf{W}_l^{\mathrm{H}}\bar{\mathbf{U}}_l^{\mathrm{H}}\mathbf{D}_l\right) \\ & + \sum_{l=1}^{L}\mathrm{tr}\left(\mathbf{W}_l^{\mathrm{H}}\mathbf{B}_l\mathbf{W}_l\right) + \sum_{t=1}^{T}\mathrm{tr}\left(\mathbf{W}_t^{\mathrm{H}}\mathbf{B}_l\mathbf{W}_t\right) \quad (37a)\end{aligned}$$

$$\text{s.t.} \quad (26b) - (26d), (26g) \quad (37b)$$

where $\mathbf{B}_k = \sum_{r=1}^{K}\bar{\mathbf{U}}_r^{\mathrm{H}}\mathbf{D}_r\mathbf{A}_r\mathbf{D}_r^{\mathrm{H}}\bar{\mathbf{U}}_r$, and $\mathbf{B}_l = \sum_{i=1}^{L}\bar{\mathbf{U}}_i^{\mathrm{H}}\mathbf{D}_i\mathbf{A}_i\mathbf{D}_i^{\mathrm{H}}\bar{\mathbf{U}}_i$.

Further, the R-EH constraint can be relaxed using successive convex approximation (SCA) as [50]

$$\begin{aligned}\mathrm{tr}\left(\sum_{k=1}^{K}\mathbf{W}_k^{\mathrm{H}}\mathbf{V}_{tm}\mathbf{W}_k\right) \geq & -\mathrm{tr}\left(\sum_{k=1}^{K}\mathbf{W}_k^{(i)\mathrm{H}}\mathbf{V}_{tm}\mathbf{W}_k^{(i)}\right) \\ & + 2\,\mathrm{Re}\left[\mathrm{tr}\left(\sum_{k=1}^{K}\mathbf{W}_k^{(i)\mathrm{H}}\mathbf{V}_{tm}\mathbf{W}_k\right)\right]. \quad (38)\end{aligned}$$

Therefore, (26c) can be recast as

$$2\,\mathrm{Re}\left[\mathrm{tr}\left(\sum\nolimits_{k=1}^{K}\mathbf{W}_k^{(i)\mathrm{H}}\mathbf{V}_{tm}\mathbf{W}_k\right)\right] \geq \tilde{V}_{\min}^{\mathrm{har}}, \forall k, \quad (39)$$

where $\mathbf{W}_k^{(i)}$ is the solution obtained at the i^{th} iteration and $\tilde{V}_{\min}^{\mathrm{har}} = \bar{V}_{\min}^{\mathrm{pow}} + \mathrm{tr}\left(\sum_{k=1}^{K}\mathbf{W}_k^{(i)\mathrm{H}}\mathbf{V}_{tm}\mathbf{W}_k^{(i)}\right)$. Likewise, the T-EH constraint in (26d) can be rewritten as

$$2\,\mathrm{Re}\left[\mathrm{tr}\left(\sum\nolimits_{l=1}^{L}\mathbf{W}_l^{(i)\mathrm{H}}\mathbf{V}_{tn}\mathbf{W}_l\right)\right] \geq \tilde{Q}_{\min}^{\mathrm{har}}, \forall l, \quad (40)$$

where $\mathbf{W}_l^{(i)}$ is the solution obtained at the i^{th} iteration and $\tilde{Q}_{\min}^{\mathrm{har}} = \bar{Q}_{\min}^{\mathrm{pow}} + \mathrm{tr}\left(\sum_{l=1}^{L}\mathbf{W}_l^{(i)\mathrm{H}}\mathbf{V}_{tn}\mathbf{W}_l^{(i)}\right)$. After doing some mathematical manipulations the non-convex constraint of the target will be transformed as shown in (41). Now, we consider optimization problem as follows:

$$\begin{aligned}\min_{\mathbf{W}} \;& \sum_{k=1}^{K}\mathrm{tr}\left(\mathbf{W}_k^{\mathrm{H}}\mathbf{B}_k\mathbf{W}_k\right) - \sum_{k=1}^{K}\mathrm{tr}\left(\mathbf{A}_k\mathbf{D}_k^{\mathrm{H}}\bar{\mathbf{U}}_k\mathbf{W}_k\right) \\ & - \sum_{k=1}^{K}\mathrm{tr}\left(\mathbf{A}_k\mathbf{W}_k^{\mathrm{H}}\bar{\mathbf{U}}_k^{\mathrm{H}}\mathbf{D}_k\right) + \sum_{l=1}^{L}\mathrm{tr}\left(\mathbf{W}_l^{\mathrm{H}}\mathbf{B}_k\mathbf{W}_l\right) \\ & + \sum_{t=1}^{T}\mathrm{tr}\left(\mathbf{W}_t^{\mathrm{H}}\mathbf{B}_k\mathbf{W}_t\right) + \sum_{l=1}^{L}\mathrm{tr}\left(\mathbf{W}_l^{\mathrm{H}}\mathbf{B}_l\mathbf{W}_l\right) \\ & - \sum_{l=1}^{L}\mathrm{tr}\left(\mathbf{A}_l\mathbf{D}_l^{\mathrm{H}}\bar{\mathbf{U}}_l\mathbf{W}_l\right) - \sum_{l=1}^{L}\mathrm{tr}\left(\mathbf{A}_l\mathbf{W}_l^{\mathrm{H}}\bar{\mathbf{U}}_l^{\mathrm{H}}\mathbf{D}_l\right) \\ & + \sum_{l=1}^{L}\mathrm{tr}\left(\mathbf{W}_l^{\mathrm{H}}\mathbf{B}_l\mathbf{W}_l\right) + \sum_{t=1}^{T}\mathrm{tr}\left(\mathbf{W}_t^{\mathrm{H}}\mathbf{B}_l\mathbf{W}_t\right) \quad (42a)\end{aligned}$$

$$\text{s.t.} \quad 2\,\mathrm{Re}\left[\mathrm{tr}\left(\sum\nolimits_{k=1}^{K}\mathbf{W}_k^{(i)\mathrm{H}}\mathbf{V}_{tm}\mathbf{W}_k\right)\right] \geq \tilde{V}_{\min}^{\mathrm{har}}, \forall k, \quad (42b)$$

$$2\,\mathrm{Re}\left[\mathrm{tr}\left(\sum\nolimits_{l=1}^{L}\mathbf{W}_l^{(i)\mathrm{H}}\mathbf{V}_{tn}\mathbf{W}_l\right)\right] \geq \tilde{Q}_{\min}^{\mathrm{har}}, \forall l, \quad (42c)$$

$$\bar{R}_t \geq R_{min}^{sens}, \quad (26b) \quad (42d)$$

Since the problem (42) is in convex form, we can use standard method like CVX [51] to solve the optimal value. However, we adapted the low-complexity iterative method to solve the problem. For that, we first introduce the Lagrangian multipliers w.r.t constraints as given in (43). By calculating the first order derivative of $\mathcal{L}(\mathbf{W}_k, \mathbf{W}_l, \lambda, \rho, \mu, \alpha)$ w.r.t zero, the optimal expression of $\mathbf{W}_k^\star$, $\mathbf{W}_l^\star$, and $\mathbf{W}_t^\star$ are derived as

$$\mathbf{W}_k^\star = (\alpha\mathbf{I} + \mathbf{B}_k + \mu\mathbf{B}_t)^\dagger(\bar{\mathbf{U}}_k^{\mathrm{H}}\mathbf{D}_k\mathbf{A}_k + \lambda\mathbf{V}_{tm}\mathbf{W}_k^{(i)}), \quad (44)$$

$$\mathbf{W}_l^\star = (\alpha\mathbf{I} + \mathbf{B}_l + \mu\mathbf{B}_t)^\dagger(\bar{\mathbf{U}}_l^{\mathrm{H}}\mathbf{D}_l\mathbf{A}_l + \rho\mathbf{V}_{tn}\mathbf{W}_l^{(i)}), \quad (45)$$

$$\mathbf{W}_t^\star = (\alpha\mathbf{I} + \mu\mathbf{B}_t + \mathbf{B}_k + \mathbf{B}_l)^\dagger(\bar{\mathbf{F}}_t^{\mathrm{H}}\mathbf{D}_t\mathbf{A}_t), \quad (46)$$

where $(\cdot)^\dagger$ represents the matrix pseudoinverse. The value of λ should be chosen for ensuring that the complementary slackness condition for constraint (39) is satisfied:

$$\lambda\left(2\,\mathrm{Re}\left[\mathrm{Tr}\left(\sum\nolimits_{k=1}^{K}\mathbf{W}_k^{(i)\mathrm{H}}\mathbf{V}_{tm}\mathbf{W}_k(\lambda)\right)\right] - \tilde{V}_{\min}^{\mathrm{har}}\right) = 0. \quad (47)$$

The complementary slackness condition guarantees that the optimal solution to the problem in (42) is achieved, and is represented by $\mathbf{W}_k^\star(0)$ for all $k \in \mathcal{K}$.

$$2\,\mathrm{Re}\left[\mathrm{Tr}\left(\sum\nolimits_{k=1}^{K}\mathbf{W}_k^{(i)\mathrm{H}}\mathbf{V}_{tm}\mathbf{W}_k(0)\right)\right] \geq \tilde{V}_{\min}^{\mathrm{har}}. \quad (48)$$

So, the optimal λ is obtained as

$$\lambda = \frac{\tilde{V}_{\min}^{\mathrm{har}} - 2\,\mathrm{Re}\left[\mathrm{Tr}\left(\sum_{k=1}^{K}\mathbf{W}_k^{(i)\mathrm{H}}\mathbf{V}_{tm}(\alpha\mathbf{I} + \mathbf{B}_k)^{-1}\bar{\mathbf{U}}_k^{\mathrm{H}}\mathbf{D}_k\mathbf{A}_k\right)\right]}{2\,\mathrm{Tr}\left(\sum_{k=1}^{K}\mathbf{W}_k^{(i)\mathrm{H}}\mathbf{V}_{tm}(\alpha\mathbf{I} + \mathbf{B}_k)^{-1}\mathbf{V}_{tm}\mathbf{W}_k^{(i)}\right)} \quad (49)$$

$$\bar{R}_t = \log|\mathbf{A}_t| - \sum_{t=1}^{T} \mathrm{tr}\left(\mathbf{W}_t^{\mathrm{H}}\mathbf{B}_t\mathbf{W}_t\right) + \sum_{t=1}^{T} \mathrm{tr}\left(\mathbf{A}_t\mathbf{D}_t^{\mathrm{H}}\bar{\mathbf{F}}_t\mathbf{W}_t\right) + \sum_{t=1}^{T} \mathrm{tr}\left(\mathbf{A}_t\mathbf{W}_t^{\mathrm{H}}\bar{\mathbf{F}}_t^{\mathrm{H}}\mathbf{D}_t\right) - \mathrm{tr}(\mathbf{A}_t) - \sigma_I^2\,\mathrm{tr}(\mathbf{A}_t\mathbf{D}_t\mathbf{D}_t^{\mathrm{H}}) - \sum_{k=1}^{K} \mathrm{tr}\left(\mathbf{W}_k^{\mathrm{H}}\mathbf{B}_t\mathbf{W}_k\right) - \sum_{l=1}^{L} \mathrm{tr}\left(\mathbf{W}_l^{\mathrm{H}}\mathbf{B}_t\mathbf{W}_l\right) + D_s \tag{41}$$

$$\mathcal{L}(\mathbf{W}_k, \mathbf{W}_l, \lambda, \rho, \mu, \alpha) = \Bigg\{ \sum_{k=1}^{K} \mathrm{tr}\left(\mathbf{W}_k^{\mathrm{H}}\mathbf{B}_k\mathbf{W}_k\right) - \sum_{k=1}^{K} \mathrm{tr}\left(\mathbf{A}_k\mathbf{D}_k^{\mathrm{H}}\bar{\mathbf{U}}_k\mathbf{W}_k\right) - \sum_{k=1}^{K} \mathrm{tr}\left(\mathbf{A}_k\mathbf{W}_k^{\mathrm{H}}\bar{\mathbf{U}}_k^{\mathrm{H}}\mathbf{D}_k\right) + \sum_{l=1}^{L} \mathrm{tr}\left(\mathbf{W}_l^{\mathrm{H}}\mathbf{B}_k\mathbf{W}_l\right) + \sum_{t=1}^{T} \mathrm{tr}\left(\mathbf{W}_t^{\mathrm{H}}\mathbf{B}_k\mathbf{W}_t\right) + \lambda\tilde{V}_{\min}^{\mathrm{har}} - 2\lambda\,\mathrm{Re}\left[\mathrm{tr}\left(\sum\nolimits_{k=1}^{K} \mathbf{W}_k^{(i)\mathrm{H}}\mathbf{V}_{tm}\mathbf{W}_k\right)\right] \Bigg\} + \Bigg\{ \sum_{l=1}^{L} \mathrm{tr}\left(\mathbf{W}_l^{\mathrm{H}}\mathbf{B}_l\mathbf{W}_l\right) - \sum_{l=1}^{L} \mathrm{tr}\left(\mathbf{A}_l\mathbf{D}_l^{\mathrm{H}}\bar{\mathbf{U}}_l\mathbf{W}_l\right) - \sum_{l=1}^{L} \mathrm{tr}\left(\mathbf{A}_l\mathbf{W}_l^{\mathrm{H}}\bar{\mathbf{U}}_l^{\mathrm{H}}\mathbf{D}_l\right) + \sum_{l=1}^{L} \mathrm{tr}\left(\mathbf{W}_l^{\mathrm{H}}\mathbf{B}_l\mathbf{W}_l\right) + \sum_{t=1}^{T} \mathrm{tr}\left(\mathbf{W}_t^{\mathrm{H}}\mathbf{B}_l\mathbf{W}_t\right) + \rho\tilde{Q}_{\min}^{\mathrm{har}} - 2\rho\,\mathrm{Re}\left[\mathrm{tr}\left(\sum\nolimits_{l=1}^{L} \mathbf{W}_l^{(i)\mathrm{H}}\mathbf{V}_{tn}\mathbf{W}_l\right)\right] \Bigg\} + \mu R_{min}^{sens} - \mu\Bigg[\log|\mathbf{A}_t| - \sum_{t=1}^{T} \mathrm{tr}\left(\mathbf{W}_t^{\mathrm{H}}\mathbf{B}_t\mathbf{W}_t\right) + \sum_{t=1}^{T} \mathrm{tr}\left(\mathbf{A}_t\mathbf{D}_t^{\mathrm{H}}\bar{\mathbf{F}}_t\mathbf{W}_t\right) + \sum_{t=1}^{T} \mathrm{tr}\left(\mathbf{A}_t\mathbf{W}_t^{\mathrm{H}}\bar{\mathbf{F}}_t^{\mathrm{H}}\mathbf{D}_t\right) - \mathrm{tr}(\mathbf{A}_t) - \sigma_I^2\,\mathrm{tr}(\mathbf{A}_t\mathbf{D}_t\mathbf{D}_t^{\mathrm{H}}) - \sum_{k=1}^{K} \mathrm{tr}\left(\mathbf{W}_k^{\mathrm{H}}\mathbf{B}_t\mathbf{W}_k\right) - \sum_{l=1}^{L} \mathrm{tr}\left(\mathbf{W}_l^{\mathrm{H}}\mathbf{B}_t\mathbf{W}_l\right) + D_s\Bigg] + \alpha\Bigg[\sum_{k=1}^{K} \mathrm{Tr}(\mathbf{W}_k\mathbf{W}_k^{\mathrm{H}}) + \sum_{l=1}^{l} \mathrm{Tr}(\mathbf{W}_l\mathbf{W}_l^{\mathrm{H}}) + \sum_{t=1}^{T} \mathrm{Tr}(\mathbf{W}_t\mathbf{W}_t^{\mathrm{H}}) - P_{max}^{DFBS}\Bigg] \tag{43}$$

Similarly, the optimal ρ can be optained as

$$\rho = \frac{\tilde{Q}_{\min}^{\mathrm{har}} - 2\,\mathrm{Re}\left[\mathrm{Tr}\left(\sum_{l=1}^{L} \mathbf{W}_l^{(i)\mathrm{H}}\mathbf{V}_{tn}(\alpha\mathbf{I} + \mathbf{B}_l)^{-1}\bar{\mathbf{U}}_l^{\mathrm{H}}\mathbf{D}_l\mathbf{A}_l\right)\right]}{2\,\mathrm{Tr}\left(\sum_{l=1}^{L} \mathbf{W}_l^{(i)\mathrm{H}}\mathbf{V}_{tn}(\alpha\mathbf{I} + \mathbf{B}_l)^{-1}\mathbf{V}_{tn}\mathbf{W}_l^{(i)}\right)} \tag{50}$$

where $\boldsymbol{\lambda}$ and $\boldsymbol{\rho}$ are used to update the constraints to find the optimal value of the problem (37).

Lemma 1. *The required power at DFBS $P_b(\alpha)$ is a monotonically decreasing function of α.*

Proof. The demonstration is analogous to the findings presented in [8]. Consequently, we have excluded this section due to spatial constraints. ■

Theorem 1. *The optimal transmit beamforming matrices obtained by **Algorithm** 1 is guaranteed to converge the KKT optimal point of the problem* (26)

Proof. The proof follows a similar approach to that in [8]. Hence, it has been omitted from our paper due to space constraints. ■

C. Optimize $\boldsymbol{\Phi}$ for obtained $\mathbf{W}$

The following section, we aim to optimize the phase-shift matrices for both R-CUs, and T-CUs, which is obtained as follows:

$$(\mathcal{P}_{2b}): \text{Find} \quad \sum_{k=1}^{K} R_k(\boldsymbol{\Phi}_r) + \sum_{l=1}^{L} R_l(\boldsymbol{\Phi}_t) \tag{51a}$$

$$\text{s.t.} \quad (26c) - (26i) \tag{51b}$$

Using (28) and (29), the problem in (51) which corresponds to the optimization of $\boldsymbol{\Theta}_r$ and $\boldsymbol{\Theta}_t$ can be reformulated by fixing

Algorithm 1 MMSE Method To Solve Problem (37)

1: **Initialize** iteration index $i = 1$, ϵ, $\mathbf{W}_k^{(i)}$, $\mathbf{W}_l^{(i)}$, and $\mathbf{W}_t^{(i)}$
2: **for** i = 1,2,... **do**
3: Compute $\{\mathbf{D}_k^{i+1}\}$, $\{\mathbf{A}_k^{i+1}\}$ and $\{\mathbf{E}_k^{i+1}\}$ for given $\mathbf{W}_k^{(i)}$ by using (31), (32) and (35), respectively.
4: Evaluate $\{\mathbf{D}_l^{i+1}\}$, $\{\mathbf{A}_l^{i+1}\}$ and $\{\mathbf{E}_l^{i+1}\}$ for given $\mathbf{W}_l^{(i)}$, using (33), (34) and (36), respectively.
5: Find the α, λ and reform $\{\mathbf{W}_k^{(i+1)}(\lambda)\}$ with (44) using $\{\mathbf{D}_k^{i+1}\}$ and $\{\mathbf{A}_k^{i+1}\}$.
6: Find the α, ρ and reform $\{\mathbf{W}_l^{(i+1)}(\rho)\}$ with (45) using $\{\mathbf{D}_l^{i+1}\}$ and $\{\mathbf{A}_l^{i+1}\}$.
7: Find the α, μ and reform $\{\mathbf{W}_t^{(i+1)}(\mu)\}$ with (46) using $\{\mathbf{D}_t^{i+1}\}$ and $\{\mathbf{A}_t^{i+1}\}$.
8: Set $i \leftarrow i + 1$.
9: **end for**
10: **Output** : $\{\mathbf{D}_k^i\}$, $\{\mathbf{D}_l^i\}$, $\{\mathbf{D}_t^i\}$, $\{\mathbf{A}_k^i\}$, $\{\mathbf{A}_l^i\}$, $\{\mathbf{A}_t^i\}$, $\mathbf{W}_k^{(i)}$, $\mathbf{W}_l^{(i)}$, and $\mathbf{W}_t^{(i)}$.

alternate variables i.e., $\{\mathbf{W}_{k_r}, \mathbf{W}_{k_t}, \mathbf{V}_{k_r}, \mathbf{V}_{k_t}, \mathbf{U}_{k_r}, \mathbf{U}_{k_t}\}$ and neglecting constant terms as

$$\min_{\boldsymbol{\Phi}_r, \boldsymbol{\Phi}_t} \quad \sum_{k=1}^{K} \Bigg\{ \mathrm{tr}\left(\mathbf{A}_k\mathbf{D}_k^{\mathrm{H}}\bar{\mathbf{U}}_k\tilde{\mathbf{W}}_r\bar{\mathbf{U}}_k^{\mathrm{H}}\mathbf{D}_k\right) - \mathrm{tr}\left(\mathbf{A}_k\mathbf{D}_k^{\mathrm{H}}\bar{\mathbf{U}}_k\mathbf{W}_k\right) - \mathrm{tr}\left(\mathbf{A}_k\mathbf{W}_k^{\mathrm{H}}\bar{\mathbf{U}}_k^{\mathrm{H}}\mathbf{D}_k\right) \Bigg\} + \sum\nolimits_{l=1}^{L} \Bigg\{ \mathrm{tr}\left(\mathbf{A}_l\mathbf{D}_l^{\mathrm{H}}\bar{\mathbf{U}}_l\tilde{\mathbf{W}}_t\bar{\mathbf{U}}_l^{\mathrm{H}}\mathbf{D}_l\right) - \mathrm{tr}\left(\mathbf{A}_l\mathbf{D}_l^{\mathrm{H}}\bar{\mathbf{U}}_l\mathbf{W}_l\right) - \mathrm{tr}\left(\mathbf{A}_l\mathbf{W}_l^{\mathrm{H}}\bar{\mathbf{U}}_l^{\mathrm{H}}\mathbf{D}_l\right) \Bigg\}$$

$$\text{s.t.} \quad (26c) - (26i), \tag{52}$$

where $\tilde{\mathbf{W}}_r = \sum_{k_r=1}^{K_r} \mathbf{W}_k\mathbf{W}_k^{\mathrm{H}}$ and $\tilde{\mathbf{W}}_t = \sum_{l=1}^{L} \mathbf{W}_l\mathbf{W}_l^{\mathrm{H}}$.

By inserting $\bar{\mathbf{U}}_k = \mathbf{U}_{k,b} + \mathbf{U}_{k,r}\boldsymbol{\Phi}\mathbf{C}_{r,b}$ into (52), we have

$$\mathbf{A}_k\mathbf{D}_k^{\mathrm{H}}\bar{\mathbf{U}}_k\tilde{\mathbf{W}}_r\bar{\mathbf{H}}_k^{\mathrm{H}}\mathbf{U}_k = \mathbf{A}_k\mathbf{D}_k^{\mathrm{H}}\mathbf{U}_{k,r}\boldsymbol{\Phi}\mathbf{C}_{r,b}\tilde{\mathbf{W}}_r\mathbf{C}_{r,b}{}^{\mathrm{H}}\boldsymbol{\Phi}^{\mathrm{H}}\mathbf{U}_{k,r}^{\mathrm{H}}\mathbf{D}_k + \mathbf{A}_k\mathbf{D}_k^{\mathrm{H}}\mathbf{U}_{k,b}\tilde{\mathbf{W}}_r\mathbf{C}_{r,b}{}^{\mathrm{H}}\boldsymbol{\Phi}^{\mathrm{H}}\mathbf{U}_{k,r}^{\mathrm{H}}\mathbf{D}_k$$

$$+\mathbf{A}_k\mathbf{D}_k^{\mathrm{H}}\mathbf{U}_{k,r}\mathbf{\Phi}\mathbf{C}_{r,b}\tilde{\mathbf{W}}_r\mathbf{U}_{k,b}^{\mathrm{H}}\mathbf{D}_k+\mathbf{A}_k\mathbf{D}_k^{\mathrm{H}}\mathbf{U}_{k,b}\tilde{\mathbf{W}}_r\mathbf{U}_{k,b}^{\mathrm{H}}\mathbf{D}_k, \tag{53}$$

and

$$\mathbf{A}_k\mathbf{D}_k^{\mathrm{H}}\bar{\mathbf{U}}_k\mathbf{W}_k=\mathbf{A}_k\mathbf{D}_k^{\mathrm{H}}\mathbf{U}_{k,r}\mathbf{\Phi}\mathbf{C}_{r,b}\mathbf{W}_k+\mathbf{A}_k\mathbf{D}_k^{\mathrm{H}}\mathbf{U}_{k,b}\mathbf{W}_k. \tag{54}$$

For notation simplicity, we define $\mathbf{F}_k \triangleq \mathbf{U}_{k,r}^{\mathrm{H}}\mathbf{D}_k\mathbf{A}_k\mathbf{D}_k^{\mathrm{H}}\mathbf{U}_{k,r}$, $\mathbf{G} \triangleq \mathbf{C}_{r,b}\tilde{\mathbf{W}}_r\mathbf{C}_{r,b}^{\mathrm{H}}$, and

$\mathbf{Z}_k \triangleq \mathbf{C}_{r,b}\tilde{\mathbf{W}}_r^{\mathrm{H}}\mathbf{U}_{k,b}\mathbf{D}_k\mathbf{A}_k\mathbf{D}_k^{\mathrm{H}}\mathbf{U}_{k,r}$. Using (53), we have

$$\begin{aligned}\mathrm{tr}\left(\mathbf{A}_k\mathbf{D}_k^{\mathrm{H}}\bar{\mathbf{U}}_k\tilde{\mathbf{W}}_r\bar{\mathbf{U}}_k^{\mathrm{H}}\mathbf{D}_k\right)=&\mathrm{tr}\left(\mathbf{\Phi}^{\mathrm{H}}\mathbf{F}_k\mathbf{\Phi}\mathbf{G}\right)+\mathrm{tr}\left(\mathbf{\Phi}^{\mathrm{H}}\mathbf{Z}_k^{\mathrm{H}}\right)\\&+\mathrm{tr}\left(\mathbf{\Phi}\mathbf{Z}_k\right)+\mathrm{c}_1,\end{aligned} \tag{55}$$

where c_1 is the independent of the $\mathbf{\Phi}$.

Likewise, we deine the $\mathbf{C}_k \triangleq \mathbf{C}_{r,b}\mathbf{W}_k\mathbf{A}_k\mathbf{D}_k^{\mathrm{H}}\mathbf{U}_{k,r}$, uisng (54), we have

$$\mathrm{tr}\left(\mathbf{A}_k\mathbf{D}_k^{\mathrm{H}}\bar{\mathbf{U}}_k\mathbf{W}_k\right)=\mathrm{tr}\left(\mathbf{\Phi}\mathbf{C}_k\right)+\mathrm{c}_2, \tag{56}$$

where c_2 is the independent of the $\mathbf{\Phi}$.

Be defining $\mathbf{V}_b = \sum_{m=1}^{M}\eta\alpha_m\mathbf{V}_{m,b}^{\mathrm{H}}\mathbf{V}_{m,b}$, $\mathbf{V}_r = \sum_{m=1}^{M}\eta\alpha_m\mathbf{V}_{m,r}^{\mathrm{H}}\mathbf{V}_{m,r}$ and

$\mathbf{V}_{br} = \mathbf{C}_{r,b}\tilde{\mathbf{W}}_r\sum_{m=1}^{M}\eta\alpha_m\mathbf{V}_{m,b}^{\mathrm{H}}\mathbf{V}_{m,r}$.

Based on above equations, the EH constraint in (26c) is recast as follows:

$$\begin{aligned}&\mathrm{tr}\left(\mathbf{\Phi}^{\mathrm{H}}\mathbf{V}_r\mathbf{\Phi}\mathbf{G}\right)+\mathrm{tr}\left(\mathbf{\Phi}^{\mathrm{H}}\mathbf{V}_{br}^{\mathrm{H}}\right)+\mathrm{tr}\left(\mathbf{\Phi}\mathbf{V}_{br}\right)\\&\quad+\mathrm{tr}\left(\mathbf{V}_b\tilde{\mathbf{W}}_r\right)\geq\bar{V}_{min}^{\mathrm{pow}}.\end{aligned} \tag{57}$$

Likewise, the EH in (26d) is rewritten as

$$\begin{aligned}&\mathrm{tr}\left(\mathbf{\Phi}^{\mathrm{H}}\mathbf{V}_t\mathbf{\Phi}\mathbf{G}_t\right)+\mathrm{tr}\left(\mathbf{\Phi}^{\mathrm{H}}\mathbf{V}_{bt}^{\mathrm{H}}\right)+\mathrm{tr}\left(\mathbf{\Phi}\mathbf{V}_{bt}\right)\\&\quad+\mathrm{tr}\left(\mathbf{V}_b\tilde{\mathbf{W}}_t\right)\geq\bar{Q}_{min}^{\mathrm{pow}}.\end{aligned} \tag{58}$$

Inserting (55) and (56) into problem (52), we have

$$\begin{aligned}\min_{\mathbf{\Phi}}\quad&\mathrm{tr}\left(\mathbf{\Phi}^{\mathrm{H}}\mathbf{F}\mathbf{\Phi}\mathbf{G}\right)+\mathrm{tr}\left(\mathbf{\Phi}^{\mathrm{H}}\mathbf{T}^{\mathrm{H}}\right)+\mathrm{tr}\left(\mathbf{\Phi}\mathbf{T}\right)\\&+\mathrm{tr}\left(\mathbf{\Phi}^{\mathrm{H}}\mathbf{F}_t\mathbf{\Phi}\mathbf{G}_t\right)+\mathrm{tr}\left(\mathbf{\Phi}^{\mathrm{H}}{\mathbf{T}_t}^{\mathrm{H}}\right)+\mathrm{tr}\left(\mathbf{\Phi}\mathbf{T}_t\right)\\\text{s.t.}\quad&(26\text{e})-(26\text{i}),(57),(58).\end{aligned} \tag{59}$$

where $\mathbf{F}$ and $\mathbf{T}$ are given by $\mathbf{F} = \sum_{k=1}^{K}\mathbf{F}_k$ and $\mathbf{T} = \sum_{k=1}^{K}\mathbf{Z}_k - \sum_{k=1}^{K}\mathbf{C}_k$.

By denoting collection of reflection elements $\mathbf{\Phi}$ by $\boldsymbol{\phi} = [\phi_1, \phi_2\cdots\phi_Z]^{\mathrm{T}}$ and adopting matrix identity [52], given by

$$\mathrm{tr}\left(\mathbf{\Phi}^{\mathrm{H}}\mathbf{F}\mathbf{\Phi}\mathbf{G}\right)=\boldsymbol{\phi}^{\mathrm{H}}\left(\mathbf{F}\odot\mathbf{G}^{\mathrm{T}}\right)\boldsymbol{\phi}, \tag{60}$$

$$\mathrm{tr}\left(\mathbf{\Phi}^{\mathrm{H}}\mathbf{V}_r\mathbf{\Phi}\mathbf{G}\right)=\boldsymbol{\phi}^{\mathrm{H}}\left(\mathbf{V}_r\odot\mathbf{G}^{\mathrm{T}}\right)\boldsymbol{\phi}. \tag{61}$$

Denoting the collection of diagonal elements of $\mathbf{T}$ and $\mathbf{V}_{br}$ as $\mathbf{t} = [[\mathbf{T}]_{1,1},\cdots,[\mathbf{T}]_{Z,Z}]^{\mathrm{T}}$ and $\mathbf{v} = [[\mathbf{V}_{br}]_{1,1},\cdots,[\mathbf{V}_{br}]_{Z,Z}]^{\mathrm{T}}$, we arrive at

$$\mathrm{tr}\left(\mathbf{\Phi}\mathbf{T}\right)=\mathbf{t}^{\mathrm{T}}\boldsymbol{\phi},\mathrm{tr}\left(\mathbf{\Phi}^{\mathrm{H}}\mathbf{T}^{\mathrm{H}}\right)=\boldsymbol{\phi}^{\mathrm{H}}\boldsymbol{t}^{*}, \tag{62}$$

$$\mathrm{tr}\left(\mathbf{\Phi}\mathbf{V}_{br}\right)=\mathbf{v}^{\mathrm{T}}\boldsymbol{\phi},\mathrm{tr}\left(\mathbf{\Phi}^{\mathrm{H}}\mathbf{V}_{br}^{\mathrm{H}}\right)=\boldsymbol{\phi}^{\mathrm{H}}\boldsymbol{v}^{*}. \tag{63}$$

Therefore, the EH constraint (57) is further transformed as

$$\boldsymbol{\phi}^{\mathrm{H}}\boldsymbol{\xi}\boldsymbol{\phi}+2\mathrm{Re}\left\{\boldsymbol{\phi}^{\mathrm{H}}\boldsymbol{v}^{*}\right\}\geq\hat{V}, \tag{64}$$

where $\hat{V}=\bar{V}_{min}^{\mathrm{pow}}-\mathrm{tr}(\mathbf{V}_b\tilde{\mathbf{W}}_r)$ and $\boldsymbol{\xi}=\mathbf{V}_r\odot\mathbf{G}^{\mathrm{T}}$, where $\mathbf{V}_r$ and $\mathbf{G}^{\mathrm{T}}$ are non-negative semidefinite matrices.

Therefore, the problem (59) is transformed as follows:

$$\min_{\boldsymbol{\phi}}\quad\boldsymbol{\phi}^{\mathrm{H}}\mathbf{\Xi}_r\boldsymbol{\phi}+2\mathrm{Re}\left\{\boldsymbol{\phi}^{\mathrm{H}}\boldsymbol{t}^{*}\right\}+\boldsymbol{\phi}^{\mathrm{H}}\mathbf{\Xi}_t\boldsymbol{\phi}+2\mathrm{Re}\left\{\boldsymbol{\phi}^{\mathrm{H}}\boldsymbol{t}_t^{*}\right\} \tag{65a}$$

$$\text{s.t.}\quad(26\text{e})-(26\text{i}),(64), \tag{65b}$$

where $\mathbf{\Xi}_r=\mathbf{F}\odot\mathbf{G}^{\mathrm{T}}$ and $\mathbf{\Xi}_t=\mathbf{F}_t\odot\mathbf{G}_t^{\mathrm{T}}$.

To handle the non-convex constraint (64), we adopt the SCA method [53].

$$\boldsymbol{\phi}^{\mathrm{H}}\boldsymbol{\xi}\boldsymbol{\phi}\geq-\boldsymbol{\phi}^{(i)\mathrm{H}}\boldsymbol{\xi}\boldsymbol{\phi}^{(i)}+2\mathrm{Re}\left[\boldsymbol{\phi}^{\mathrm{H}}\boldsymbol{\xi}\boldsymbol{\phi}^{(i)}\right], \tag{66}$$

where $\boldsymbol{\phi}^{(i)}$ is obtained in the previous iteration. Then, the constraint (64) is replaced with the following expression.

$$2\,\mathrm{Re}\left[\phi^{\mathrm{H}}\left(\mathbf{v}^{*}+\mathbf{\Upsilon}\phi^{(i)}\right)\right]\geq\widehat{V}+\boldsymbol{\phi}^{(i)}\boldsymbol{\xi}\boldsymbol{\phi}^{(i)}, \tag{67}$$

Therefore, the problem (65) can be recast as follows:

$$\min_{\boldsymbol{\phi}}\quad\boldsymbol{\phi}^{\mathrm{H}}\mathbf{\Xi}_r\boldsymbol{\phi}+2\mathrm{Re}\left\{\boldsymbol{\phi}^{\mathrm{H}}\boldsymbol{t}^{*}\right\}+\boldsymbol{\phi}^{\mathrm{H}}\mathbf{\Xi}_t\boldsymbol{\phi}+2\mathrm{Re}\left\{\boldsymbol{\phi}^{\mathrm{H}}\boldsymbol{t}_t^{*}\right\} \tag{68a}$$

$$\text{s.t.}\quad(26\text{e})-(26\text{i}),(67) \tag{68b}$$

To obtain the optimal value of the phase-shift, we adopt majorization-minimization (MM) algorithm [54] for solving problem (68), which satisfies the following conditions:

$$\begin{aligned}&1)v(\boldsymbol{\phi}^{(i)}|\boldsymbol{\phi}^{(i)})=R(\boldsymbol{\phi}^{(i)});\\&2)\,\nabla_{\boldsymbol{\phi}^{*}}v(\boldsymbol{\phi}|\boldsymbol{\phi}^{(i)})\Big|_{\boldsymbol{\phi}=\boldsymbol{\phi}^{(i)}}=\nabla_{\boldsymbol{\phi}^{*}}R(\boldsymbol{\phi})|_{\boldsymbol{\phi}=\boldsymbol{\phi}^{(i)}};\\&3)v(\boldsymbol{\phi}|\boldsymbol{\phi}^{(i)})\geq R(\boldsymbol{\phi}).\end{aligned} \tag{69}$$

The following inequality holds for any feasible $\boldsymbol{\phi}$

$$\begin{aligned}\boldsymbol{\phi}^{\mathrm{H}}\mathbf{\Xi}\boldsymbol{\phi}\leq&\boldsymbol{\phi}^{\mathrm{H}}\mathbf{M}\boldsymbol{\phi}-2\mathrm{Re}\left\{\boldsymbol{\phi}^{\mathrm{H}}\left(\mathbf{M}-\mathbf{\Xi}\right)\boldsymbol{\phi}^{(i)}\right\}\\&+\left(\boldsymbol{\phi}^{(i)}\right)^{\mathrm{H}}\left(\mathbf{M}-\mathbf{\Xi}\right)\boldsymbol{\phi}^{(i)}\triangleq y(\boldsymbol{\phi}|\boldsymbol{\phi}^{(i)}),\end{aligned} \tag{70}$$

where $\mathbf{M}=\lambda_{\max}\mathbf{I}_Z$ and $\lambda_{\max}$ is the maximum eigenvalue of $\mathbf{\Xi}$.

Then, the function is written as

$$v(\boldsymbol{\phi}|\boldsymbol{\phi}^{(i)})=y(\boldsymbol{\phi}|\boldsymbol{\phi}^{(i)})+2\mathrm{Re}\left\{\boldsymbol{\phi}^{\mathrm{H}}\mathbf{t}^{*}\right\}, \tag{71}$$

The problem (68) is rewritten as

$$\min_{\boldsymbol{\phi}}\quad v(\boldsymbol{\phi}|\boldsymbol{\phi}^{(i)}) \tag{72a}$$

$$\text{s.t.}\quad(26\text{e}),(26\text{f}),(67). \tag{72b}$$

Since $\boldsymbol{\phi}\boldsymbol{\phi}^{\mathrm{H}}=Z$. we have $\boldsymbol{\phi}\mathbf{M}\boldsymbol{\phi}^{\mathrm{H}}=Z\lambda_{\max}$. After removing constants, the problem (72) is rewritten as

$$\max_{\boldsymbol{\phi}}\quad2\mathrm{Re}\left\{\boldsymbol{\phi}^{\mathrm{H}}\mathbf{p}_r{}^{(i)}\right\}+2\mathrm{Re}\left\{\boldsymbol{\phi}^{\mathrm{H}}\mathbf{p}_t{}^{(i)}\right\} \tag{73a}$$

$$\text{s.t.}\quad(26\text{e}),(26\text{f}),(67), \tag{73b}$$

where $\mathbf{p}_r^{(i)}=(\lambda_{\max}\mathbf{I}_Z-\mathbf{\Xi}_r)\boldsymbol{\phi}_r^{(i)}-\mathbf{t}_r^{*}$ and $\mathbf{p}_t^{(i)}=(\lambda_{\max}\mathbf{I}_Z-\mathbf{\Xi}_t)\boldsymbol{\phi}_t^{(i)}-\mathbf{t}_t^{*}$. The optimal solution for the problem in (73) cannot be derived directly as in [27] due to the inclusion of the additional constraint (67). Since the dual gap is non-zero, the Lagrangian dual decomposition approach, which is

Algorithm 2 SCA-Based Design for STAR-RIS to Solve Problem (51)

1: Initialize $R_r(\boldsymbol{\phi}_r^{(1)})$, $R_t(\boldsymbol{\phi}_t^{(1)})$, iteration index $i=1$ and $i_{\max}$.
2: Compute $\widehat{V}+\boldsymbol{\phi}^{(i)}\boldsymbol{\xi}\boldsymbol{\phi}^{(i)}$ using (67).
3: Compute $\mathbf{p}_r^{(i)}=(\lambda_{\max}\mathbf{I}_Z-\boldsymbol{\Xi}_r)\boldsymbol{\phi}_r^{(i)}-\mathbf{t}_r^*$ and $\mathbf{p}_t^{(i)}=(\lambda_{\max}\mathbf{I}_Z-\boldsymbol{\Xi}_t)\boldsymbol{\phi}_r^{(i)}-\mathbf{t}_t^*$ using (73).
4: **for** i =1,2, … **do**
5: Obtain the values of s and b using (77).
6: Set $i\leftarrow i+1$
7: Find $R_r(\boldsymbol{\Phi}_r^{(i+1)})$ and $f_t(\boldsymbol{\Phi}_t^{(i+1)})$ using (73).
8: **end for**
9: Calculate $\boldsymbol{\Phi}_r$ and $\boldsymbol{\Phi}_t$ with $\boldsymbol{\phi}_r^{(i+1)}$ and $\boldsymbol{\phi}_t^{(i+1)}$.
10: Optimal : $\boldsymbol{\Phi}_r$ and $\boldsymbol{\Phi}_t$.

effective for the convex problem in (42), is not applicable in this case. To tackle Problem (73), we propose a pricing mechanism to obtain a globally optimal solution. By introducing a non-negative price variable s and b on the left-hand side of constraint (73), we reformulate the problem and solve it accordingly.

$$\begin{aligned}\max_{\boldsymbol{\phi}} \quad & 2\,\mathrm{Re}\{\boldsymbol{\phi}_r^{\mathrm{H}}\mathbf{p}_r^{(i)}\}+2s\,\mathrm{Re}\left[\phi^{\mathrm{H}}\left(\mathbf{v}^*+\boldsymbol{\Upsilon}\phi^{(i)}\right)\right]\\ & +2\,\mathrm{Re}\{\boldsymbol{\theta}_t^{\mathrm{H}}\mathbf{p}_t^{(n)}\}+2b\,\mathrm{Re}\left[\phi^{\mathrm{H}}\left(\mathbf{v}_t^*+\boldsymbol{\Upsilon}_t\phi^{(i)}\right)\right]\\ \text{s.t} \quad & (26e),(26f). \end{aligned} \tag{74}$$

The optimal solution is obtained by as

$$\boldsymbol{\phi}(s)=e^{j\arg\left(\mathbf{p}_r^{(i)}+s\left(\mathbf{v}^*+\boldsymbol{\Upsilon}\boldsymbol{\phi}_r^{(i)}\right)\right)}, \tag{75}$$

$$\boldsymbol{\phi}(b)=e^{j\arg\left(\mathbf{p}_t^{(i)}+b\left(\mathbf{v}_t^*+\boldsymbol{\Upsilon}_t\boldsymbol{\phi}_t^{(i)}\right)\right)}, \tag{76}$$

By obtaining complementary slackness condition to solve constraint s and b is given by

$$s\left(X(s)-\widehat{V}+\boldsymbol{\phi}^{(i)}\boldsymbol{\xi}\boldsymbol{\phi}^{(i)}\right)=0, \tag{77}$$

where $X(s)=2\,\mathrm{Re}\left[\phi(s)^{\mathrm{H}}\left(\mathbf{v}^*+\boldsymbol{\Upsilon}\phi^{(i)}\right)\right]$. The following two conditions are used to solve the above equation.
Condition I: In this condition, if $s=0$

$$\boldsymbol{\phi}(0)=\begin{cases}e^{j\arg\left(\mathbf{p}_r^{(i)}\right)}, & \text{yields the constraint (67),}\\ s>0, & \text{otherwise.}\end{cases}$$

Condition II: In this condition, if $s>0$, solving (77) holds

$$X(s)=\widehat{V}+\boldsymbol{\phi}^{(i)}\boldsymbol{\xi}\boldsymbol{\phi}^{(i)}. \tag{78}$$

The function $X(s)$ increases uniformly w.r.t s, ensuring its convergence. Similarly, we solve the complementary slackness condition for transmission phase-shift. The complete procedure for addressing the STAR-RIS phase-shift beamforming design is outlined in **Algorithm 2**.

Lemma 2. *$X(s)$ increases uniformly w.r.t. s.*

Proof. The proof follows a similar approach in **Lemma 1** and is therefore omitted for the sake of space brevity. ■

Theorem 2. *The optimal values obtained by the Algorithm 3 is guaranteed to converge, and satisfies the KKT conditions of Problem 8.*

Algorithm 3 Proposed AO Algorithm

1: Initialize $i=1$, $\mathbf{W}^{(1)}$, $\boldsymbol{\Phi}^{(1)}$, ε.
2: Evaluate $\mathbf{D}_r^{(1)}$ and $\mathbf{D}_t^{(1)}$ using (31) and (33),
3: Evaluate $\mathbf{A}_r^{(1)}$ and $\mathbf{A}_t^{(1)}$ using (32) and (34),
4: **for** i=1,2,… **do**
5: Find the transmit precoder matrices ($\mathbf{W}_r^{(i+1)}$, $\mathbf{W}_t^{(i+1)}$) for given $\mathbf{D}_r^{(1)}$, $\mathbf{D}_t^{(1)}$, $\mathbf{A}_r^{(1)}$ and $\mathbf{A}_t^{(1)}$ by relaxing problem (37) with **Algorithm** 1.
6: Find the phase-shift matrices ($\boldsymbol{\Phi}_r^{(i+1)}$, $\boldsymbol{\Phi}_t^{(i+1)}$) for given $\mathbf{D}_r^{(1)}$, $\mathbf{D}_t^{(1)}$, $\mathbf{A}_r^{(1)}$, $\mathbf{A}_t^{(1)}$, $\mathbf{W}_r^{(i+1)}$ and $\mathbf{W}_t^{(i+1)}$ by solving problem (51) using Algorithm 2.
7: Correct the optimal values of $\mathbf{D}_r^{(i+1)}$, $\mathbf{D}_t^{(i+1)}$ and $\mathbf{A}_r^{(i+1)}$, $\mathbf{A}_t^{(i+1)}$ using $\mathbf{W}_r^{(i+1)}$, $\mathbf{W}_t^{(i+1)}$, $\boldsymbol{\Phi}_t^{(i+1)}$ and $\boldsymbol{\Phi}_r^{(i+1)}$.
8: $i\leftarrow i+1$,
9: **end for**
10: OutPut : $\mathbf{W}_k, \mathbf{W}_l, \boldsymbol{\Phi}_r$, and $\boldsymbol{\Phi}_t$

Proof. The proof follows the same method as in [8, **Algorithm 5**] and is omitted here due to space constraints. ■

D. Joint Solution and Computational Complexity

We present a joint solution using an proposed AO framework, as outlined in **Algorithm** 3. Specifically, this approach tackles the sub-problems of sum-rate maximization for ISAC systems by enhancing the transmit beamforming design at the DFBS and passive beamforming design at the STAR-RIS, both subject to given Quality of Service (QoS) constraints. Starting with an initial or randomly chosen precoder matrix and beamforming design, each sub-problem is solved iteratively. Crucially, the output from one sub-problem in each iteration is used as the input for the other sub-problem in the subsequent iteration. In this iterative process, the updated precoder at the DFBS and the passive beamforming matrices at the STAR-RIS from the previous iteration are used to reevaluate all parameters. This procedure is repeated until a stationary point in the sum-rate is achieved.

Next, we present the complete computational complexity of the proposed and benchmarking schemes. Let us assume the parameters $N_B > K > L > T > D_s$ to calculate the complexity of the transmit beamforming matrices. The main complexity of the **Algorithm** 1 in every iteration lies in achieving the $\mathbf{W}_k^{(i+1)}, \forall k$, $\mathbf{W}_l^{(i+1)}, \forall l$, and $\mathbf{W}_t^{(i+1)}, \forall t$ by using the alternate optimization method mentioned in **Algorithm** 1. The main computational complexity lies in solving equations (44), (45), and (46). The overall iteration required for the **Algorithm** 1 to converge is given by $\left(\frac{\alpha_{upp}-\alpha_{low}}{\epsilon}\right)$, and $\left(\frac{t_{upp}-t_{low}}{\epsilon}\right)$. Similarly, the complexity of the **Algorithm** 2 is defined by $\mathcal{O}(Z^3)$ and $\mathcal{O}(N_{Ra}^3)$ for the STAR-RIS and A-RIS, respectively. The iteration index to converge overall **Algorithm** 2 is given by $\left(\frac{s_{upp}-s_{low}}{\epsilon}\right)$, and $\left(\frac{a_{upp}-a_{low}}{\epsilon}\right)$. Therefore, the total complexity of the **Algorithm** 3 is defined by

$$\mathcal{O}\left(i_{\max}\left(i_1^{\max}\log_2\left(\frac{\alpha_{upp}-\alpha_{low}}{\epsilon}\right)KLN_B^3\right.\right.$$

TABLE II: Complexity of benchmarking schemes

Scheme	Complexity
Scheme 1	$\mathcal{O}\left(i_{\max}\left(i_1^{\max}\log_2\left(\frac{\alpha_{upp}-\alpha_{low}}{\epsilon}\right)KLN_B^3+i_2^{\max}\log_2\left(\frac{s_{upp}-s_{low}}{\epsilon}\right)Z^3+i_3^{\max}\log_2\left(\frac{t_{upp}-t_{low}}{\epsilon}\right)T+i_4^{\max}\log_2\left(\frac{a_{upp}-a_{low}}{\epsilon}\right)N_{R_a}^3\right)\right)$
Scheme 2	$\mathcal{O}\left(i_{\max}\left(i_1^{\max}\log_2\left(\frac{\alpha_{upp}-\alpha_{low}}{\epsilon}\right)KLN_B^3+i_2^{\max}\log_2\left(\frac{s_{upp}-s_{low}}{\epsilon}\right)Z^3/2+i_3^{\max}\log_2\left(\frac{t_{upp}-t_{low}}{\epsilon}\right)T+i_4^{\max}\log_2\left(\frac{a_{upp}-a_{low}}{\epsilon}\right)N_{R_a}^3\right)\right)$
Scheme 3	$\mathcal{O}\left(i_{\max}\left(i_1^{\max}\log_2\left(\frac{\alpha_{upp}-\alpha_{low}}{\epsilon}\right)KLN_B^3+i_3^{\max}\log_2\left(\frac{t_{upp}-t_{low}}{\epsilon}\right)T+i_4^{\max}\log_2\left(\frac{a_{upp}-a_{low}}{\epsilon}\right)N_{R_a}^3\right)\right)$
Scheme 4	$\mathcal{O}\left(i_{\max}\left(i_1^{\max}\log_2\left(\frac{\alpha_{upp}-\alpha_{low}}{\epsilon}\right)KLN_B^3+N_T^3KLT+i_3^{\max}\log_2\left(\frac{t_{upp}-t_{low}}{\epsilon}\right)T\right)\right)$
Scheme 5	$\mathcal{O}\left(Z^3+KLN_B^3\log_2(1/\epsilon)+N_{R_a}^3+T\log_2(1/\epsilon)\right)$

TABLE III: System parameters.

Symbol	Value	Symbol	Value	Symbol	Value	Symbol	Value
$\mathbf{C}_{r,b}$	2.2	$\mathbf{V}_{m,r}$	2.2	N_B	4	$\bar{V}_{\min}^{\text{pow}}$	2×10^{-4} W,
$\mathbf{U}_{k,b}$	2.4	$\mathbf{U}_{k,r}$	3.6	$N_{I_r}=N_{I_t}$	2	$\bar{Q}_{\min}^{\text{pow}}$	1.5×10^{-4} W.
$\mathbf{V}_{m,b}$	3.4	$\mathbf{V}_{n,r}$	3.4	L	3	M	4
$\mathbf{U}_{l,r}$	3.3	$\mathbf{F}$	4.2	$N_{E_r}=N_{E_t}$	2	N	4
$\mathbf{F}_{t,b}$	3.6	$\mathbf{F}_{t,r}$	4.3	Z	18	K	3
P_{max}^{A-RIS}	4.15 dB	W_1	7 dBm	W_2	7 dBm	N_{R_a}	24

$$+i_2^{\max}\log_2\left(\frac{s_{upp}-s_{low}}{\epsilon}\right)Z^3+i_3^{\max}\log_2\left(\frac{t_{upp}-t_{low}}{\epsilon}\right)T+i_4^{\max}\log_2\left(\frac{a_{upp}-a_{low}}{\epsilon}\right)N_{R_a}^3\Bigg)\Bigg),$$

where $i_{\max}$ is the maximum iterative index of the **Algorithm** 3 to converge. In similar way, we can derive the complexity analysis of the benchmarking schemes which are presented in the **Table II**.

V. Simulation Outcomes and Discussion

In this section, we describe the simulation results for the proposed algorithm within the STAR-RIS and A-RIS assisted ISAC SWIPT framework [28]. The parameter settings of the proposed algorithm are defined in **Table III**.

A. Channel Model

The large-scale path loss is modeled in dB as

$$PL = PL_s\left(D_s\Big/D_{s_0}\right)^{-\alpha}, \tag{79}$$

where $PL_s = -30$ dB is the path loss at the reference distance $D_{s_0}=1$ m and α is the path loss exponent. The path loss exponent for DFBS-STAR-RIS, STAR-RIS-R-ED, STAR-RIS-R-CU, DFBS-R-CU, STAR-RIS-T-ED, STAR-RIS-T-CU and DFBS- R-ED communication links are given in Table III. Moreover, the minor fluctuations in signal strength across all connections to the STAR-RIS adhere to the Rician fading statistical model. [8], [28]. For instance, the channels from STAR-RIS to R-ED are denoted as:

$$\tilde{\mathbf{V}}_{m,r}=\sqrt{\frac{\beta_{\mathrm{V}_{m,r}}}{\beta_{\mathrm{V}_{m,r}}+1}}\tilde{\mathbf{V}}_{m,r}^{\mathrm{LoS}}+\sqrt{\frac{1}{\beta_{\mathrm{V}_{m,r}}+1}}\tilde{\mathbf{V}}_{m,r}^{\mathrm{NLoS}},\forall m \tag{80}$$

where $\beta_{\mathrm{V}_{m,r}}$ is the Rician factor, $\tilde{\mathbf{V}}_{m,r}^{\mathrm{LoS}}$ and $\tilde{\mathbf{V}}_{m,r}^{\mathrm{NLoS}}$ are the LoS (deterministic) and NLoS (Rayleigh) components. The deterministic LoS component $\tilde{\mathbf{V}}_{m,r}^{\mathrm{LoS}}$ is expressed as $\tilde{\mathbf{V}}_{m,r}^{\mathrm{LoS}}=\mathbf{a}_{N_{E_r}}\left(\vartheta^{AoA}\right)\mathbf{a}_Z^H\left(\vartheta^{AoD}\right)$, where $\mathbf{a}_{N_{E_r}}\left(\vartheta^{AoA}\right)$ and $\mathbf{a}_Z\left(\vartheta^{AoD}\right)$ is defined as

$$\mathbf{a}_{N_{E_r}}\left(\vartheta^{AoA}\right)=\left[1,e^{j\frac{2\pi d}{\lambda}\sin\vartheta^{AoA}},\cdots,e^{j\frac{2\pi d}{\lambda}(N_{E_r}-1)\sin\vartheta^{AoA}}\right]^T \tag{81}$$

$$\mathbf{a}_Z\left(\vartheta^{AoD}\right)=\left[1,e^{j\frac{2\pi d}{\lambda}\sin\vartheta^{AoD}},\cdots,e^{j\frac{2\pi d}{\lambda}(Z-1)\sin\vartheta^{AoD}}\right]^T, \tag{82}$$

where d represents the spatial separation distance between antennas and λ denotes the wavelength (we establish $d/\lambda = 1/2$). The parameters ϑ^{AoD} and ϑ^{AoA} correspond to the angle of departure and angle of arrival, respectively, and it is postulated that these angles are uniformly distributed over the interval $[0, 2\pi]$. The components of $\tilde{\mathbf{V}}_{m,r}$ are subsequently scaled by the square root of the large-scale path loss as delineated in (53). In a similar vein, the small-scale fading phenomena from the DFBS to the STAR-RIS and the EDs conform to a Rician model. The small-scale fading associated with the direct transmission channel from BS to the R-IRs, as well as the reflected link from the STAR-RIS to the R-IRs and T-IRS, adheres to a Rayleigh distribution [8]. For all Rician fading channels discussed here, the parameter value is $\beta = 3$. For instance, the channels from A-RIS to targets and DFBS to targets are are denoted as:

$$\tilde{\mathbf{F}}_{t,r}[n]=e^{j2\pi f_d[n-1]}\sqrt{\frac{\beta_{\mathrm{F}_{t,r}}}{\beta_{\mathrm{F}_{t,r}}+1}}\tilde{\mathbf{F}}_{t,r}^{\mathrm{LoS}}+\sqrt{\frac{1}{\beta_{\mathrm{F}_{t,r}}+1}}\tilde{\mathbf{F}}_{t,r}^{\mathrm{NLoS}},\forall t \tag{83}$$

where f_d represents the doppler shift such as $f_d = \mathcal{V}cos(\alpha_{AoA})cos(\eta_{AoA})/\lambda$, $\mathcal{V}$ is the speed of the target in meters/second, λ is the signal wavelength and α_{AoA}, η_{AoA} are assumed to be azimuth and elevation angles. Similarly, we define the channel between DFBS and targets. Hence, we removed due to space brevity.

B. Benchmarking Schemes

The benchmarking schemes used against proposed algorithm are defined as follows:

This article has been accepted for publication in IEEE Transactions on Cognitive Communications and Networking. This is the author's version which has not been fully edited and content may change prior to final publication. Citation information: DOI 10.1109/TCCN.2025.3543405

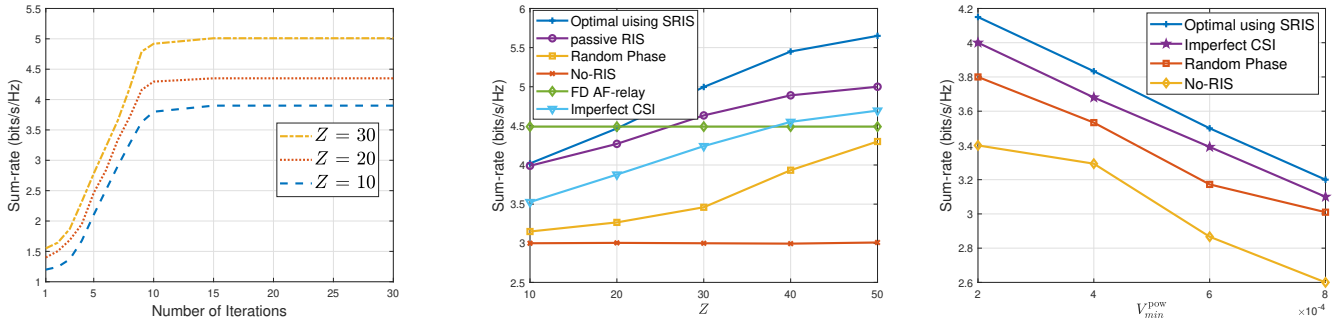

Fig. 2: a) Convergence behavior of **Algorithm 3** b) Impact of STAR-RIS elements and c) Impact of R-ED threshold.

- *Scheme 1:* This scheme shows the performance of the STAR-RIS on the ISAC SWIPT systems.
- *Scheme 2:* For the purpose of performance benchmarking and comparative analysis, we also evaluated the STAR-RIS against the traditional passive RIS $(Z/2)$ elements, are positioned in the exact place as the STAR-RIS, with one RIS reflecting the incident signal towards the reflection users and the other reflecting towards the transmission users [44].
- *Scheme 3:* The proposed algorithm is compared with No-RIS (where $Z = 0$).
- *Scheme 4:* In this scheme, the amplify-forward (AF) relay is used to show the performance of the STAR-RIS.
- *Scheme 5:* Finally, we compare the proposed STAR-RIS ISAC SWIPT system with the channel estimation errors.

C. Convergence

Initially, we examine the convergence performance of the proposed solution presented in **Algorithm 3**, for the STAR-RIS ISAC-assisted SWIPT. As depicted in Fig. 2a, it clearly states that the system reaches a stable point after 7-10 iterations. It is noteworthy that **Algorithm 3** begins with random precoding initially at the DFBS, and optimize the signal ensuring that the QoS requirements for the system constraints. Notably, the proposed approach achieves a maximum beamforming gain while increase in number of STAR-RIS elements. Finally, it is evident that increasing the number of STAR-RIS elements leads to further increase in communication sum-rate by suppressing the interference form the SWIPT and sensing systems.

D. Impact of STAR-RIS elements Z and FD AF-relay

Fig. 2b presents a comparable performance evaluation of the proposed STAR-RIS ISAC-aided SWIPT against various benchmarking methods for different numbers of STAR-RIS elements Z. Intuitively, with the increase in STAR-RIS elements, the available phase shifters also increase, that enhances channel gain diversity for each user, resulting in a rate requirement to meet the specified QoS under both perfect and imperfect CSI conditions. The STAR-RIS, which works in energy splitting mode provides 360° coverage compared to conventional passive RIS models. However, the system's performance is more sensitive to imperfect CSI (i-CSI), which degardes the rate requirements towards the users than perfect CSI (p-CSI). For example, the optimal with STAR-RIS using perfect CSI requires approximately 5.6 (bits/s/Hz), while STAR-RIS-SWIPT i-CSI requires the 4.7 (bits/s/Hz) of rate to satisfy the desired QoS when $Z = 50$. Additionally, we plot the sum-rate maximization (transmission power + amplification power) required when a full-duplex amplify-and-forward AF-relay, as described in [55], with 3 transmit and 3 receive antennas, is used instead of an STAR-RIS. It is evident that, similar to the scenario without an RIS, the performance remains unaffected by Z in this scheme. Moreover, the rate required for the FD AF-relay setup is higher than the No-RIS scheme. Despite that, there is a intersection between the performance of the FD AF-relay and STAR-RIS-SWIPT-pCSI, STAR-RIS-SWIPT-iCSI, and passive RIS when $Z \geq 20$. Specifically, the FD-AF relay outperforms when $Z \leq 20$, while the Optimal STAR-RIS scheme outperforms it for $Z \geq 20$ due to higher beamforming gains. It is also noteworthy that the rate difference between optimal STAR-RIS scheme and the FD AF-relay is smaller for lower values of Z, whereas the Optimal scheme shows a significant increase in rate as Z increases. Thus, for the given parameter set, by tuning the number of STAR-RIS elements, the proposed algorithm significantly enhances rate maximization compared to other approaches.

E. Effect of R-ED Threshold with fixed T-ED

In Fig. 2c, we illustrate the effect of the minimum harvested power requirement at EH $\bar{V}_{min}^{\text{pow}}$ at the R-EDs while fixing T-EDs threshold on the sum-rate necessary to achieve a QoSs requirements at each CUs, using $Z = 18$. The graph shows rate as a function of $\bar{V}_{min}^{\text{pow}}$ for all four scenarios. It is evident that rate function decrease as $\bar{V}_{min}^{\text{pow}}$ rises across all schemes. This behavior is explained by constraint (26c), as with fixed parameters $(N_B, Z, \bar{Q}_{\min}^{\text{pow}})$, the DFBS is required to use more power to meet higher $\bar{V}_{\min}^{\text{pow}}$ demands and satisfy the EDs minimum power requirements. However, we compared to the No-RIS scheme, the Optimal scenario demonstrates superior performance throughout the entire range of $(\bar{V}_{min}^{\text{pow}}$. For instance, the Optimal scheme achieves the higher rate with 6-10% compared to other schemes. Additionally, we examine the effect of imperfect CSI on the sum-rate to assure $\bar{V}_{\min}^{\text{pow}}$

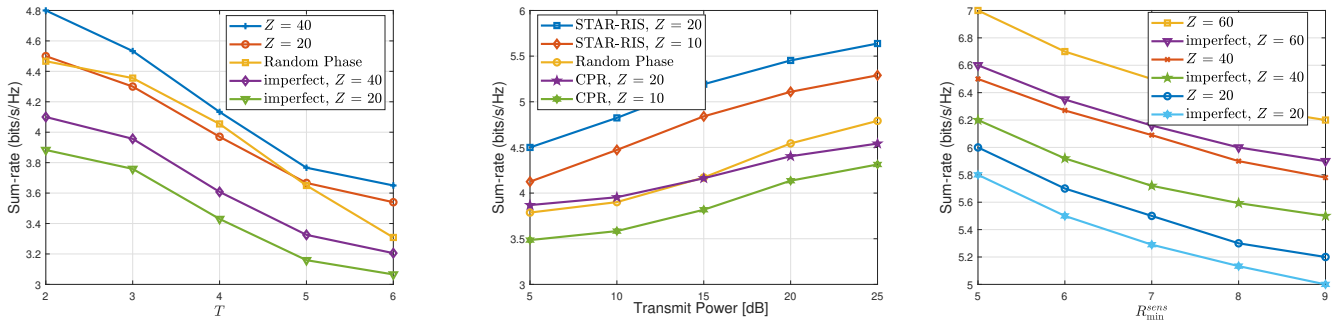

(a) **(b)** **(c)**

Fig. 3: a) Impact of number of STs b) Sum-rate vs transmit power and c) Impact of STs threshold.

at each R-ED. As expected, due to the reduction in overall channel gain at each CU, the DFBS required more transmit power to meet the QoS requirements in the imperfect CSI scenario compared to the perfect CSI scheme.

F. Effect of STs

In Fig. 3a, we show the performance of the sensing targets (STs) within the communication SWIPT system. As expected, with increase in the number of STs directs to a reduction in the communication rate, primarily due to the rise in interference. However, we also observe that the communication rate improves as the number of STAR-RIS elements increases. This clearly demonstrates that adding more STAR-RIS elements helps to effectively mitigate interference and enhance system performance. For example, at $T = 6$, the rate achieved is 3.7 bits/s/Hz with $Z = 60$ STAR-RIS elements, compared to 3.5 bits/s/Hz with fewer elements. Moreover, we compare the performance of the optimal phase design with that of a random phase configuration, holding $Z = 30$. The results show a crossover point between the random phase and optimal phase schemes when $Z = 20$. Beyond this point, as the number of STAR-RIS elements increases, the optimal phase design performs better than the random phase scheme. This highlights the significance of optimizing the phase shifts to fully leverage the advantages offered by the additional STAR-RIS elements. Moreover, we also compared the channel estimation errors over known channel, as predicted the ISAC performance degrade due to noise added to the channels. However, we observe that, the increase in STAR-RIS elements boost the overall ISAC system, even in the presence of channel errors. The substantial improvement in communication rate with more STAR-RIS elements under the optimal design further highlights its effectiveness in managing interference and boosting overall system efficiency in the presence of sensing targets.

G. Sum-rate vs Transmit Power

In Fig. 3b, we investigate the performance of the maximum transmit power P_{max}^{DFBS} available at the DFBS on the beamforming gain for different schemes, with the results shown for two distinct values of STAR-RIS elements Z and random-phase. As expected, the average beamforming gain improves as the maximum transmit power increases for each Z, reflecting the system's enhanced ability to focus energy towards the intended directions. Notably, $Z = 20$ demonstrates a significantly higher performance compared to both $Z = 10$ and the random phase design, highlighting the importance of increasing the number of STAR-RIS elements to improve beamforming precision and overall system effectiveness. Moreover, the results indicates that after a certain threshold of P_{max}^{DFBS}, the power requirements for the optimal phase designs converge, becomes constant. This suggests that beyond this point, additional transmit power no longer contributes to further performance gains, as the beamforming capability saturates. Therefore, careful selection of P_{max}^{DFBS} is crucial to ensure efficient use of power resources, avoiding excessive energy consumption without any corresponding increase in system performance. This observation also highlights an important design consideration: increasing the number of STAR-RIS elements can help achieve higher beamforming gains at lower transmit power levels, thereby improving energy efficiency. By balancing the STAR-RIS elements and the DFBS incident power, system designers can optimize the trade-off between power usage and communication quality, ensuring optimal performance while minimizing power wastage. This insight is particularly useful for applications where energy efficiency is a priority, such as in low-power communication systems or energy-constrained environments.

H. Impact of ST Threshold

Furthermore, in Fig. 3c illustrates the impact of the sensing threshold on the performance of the communication SWIPT system. As the sensing threshold $R_{\min}^{sens}$ increases, the communication beamforming gain decreases. This is due to the higher sensing QoS requirements, which necessitate more transmit power to meet the increased demands. As a point of comparison, we evaluated different numbers of STAR-RIS elements and observed that increasing the number of STAR-RIS elements leads to a corresponding rise in communication beamforming gain, even as increase in $R_{\min}^{sens}$. For instance, when $R_{\min}^{sens} = 9$, the beamforming gain achieved is 6.2, 5.8, and 5.2 bits/s/Hz with STAR-RIS configurations of 60, 40, and 20 elements, respectively. This clearly demonstrates that a careful selection of STAR-RIS elements significantly enhances communication beamforming gain while adhering to the target

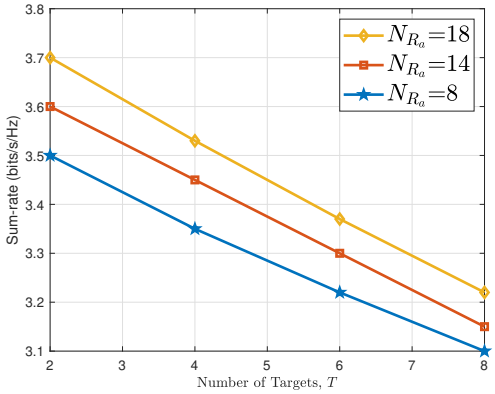

Fig. 4: Impact of doppler shift on the sum-rate.

constraints. We also compared the channel estimations as an bench marking scheme for the sensing threshold. As, expected, the increase in channel error leads to decrease in the sum-rate of the communication system due to increase in interference noise. At the same time, we can also see the increase in STAR-RIS elements will provide the additional beamforming strength to the ISAC receivers. Thus, increasing the number of STAR-RIS elements not only improves system performance but also allows for more efficient balancing of communication and sensing requirements, ensuring optimal resource allocation in SWIPT systems.

I. Impact of Doppler Shift

Finally, Fig. 4, we illustrate the effect of the doppler shift by increasing the number of targets on the communication system. As expected, the sum-rate of the communication system degraded when we increase the number targets w.rt doppler shift. As the number of doppler targets increases the interference at the communication also increase which makes the transmit signal weaker. At the same time can also see that by increasing the number RIS elements, increases the sum-rate of the communication system providing extra degree of freedom through the communication users. Finally, we can say the RIS plays the important role on both ISAC-aided SWIPT systems.

VI. Conclusion

This paper investigates the performance of communication rate by cooperatively optimizing the beamforming vector at the DFBS transmitter and phase shift matrix at the RISs under the constraint of energy harvesting, maximum power at the DFBS and A-RIS, STAR-RIS phase shift coefficients. We formulated and solved a joint optimization problem to maximize the communication rate while balancing the target rate using A-RIS which implies the trade-offs between target sensing accuracy and communication performance, demonstrating the potential of RIS to enhance system capabilities in diverse ISAC scenarios. The problem formulated in the ISAC-aided SWIPT system is jointly non-convex and NP-hard to solve. Therefore, we adopt the MMSE method to transform the original problem into its equivalent sub-problems and solve each sub-problem separately in a iterative manner. Simulation results confirmed that the proposed unified solution converged within 7-10 iterations. Additionally, the STAR-RIS SWIPT framework significantly increases the beamforming gain by 12-15% compared to traditional RIS systems that only reflect signals, this methodology fulfills the specified QoS requirements for an ISAC-assisted SWIPT system. Given the notable advantages of STAR-RIS over traditional RIS, future research could focus on the robust evaluation performance of the STAR-RIS-assisted ISAC-assisted SWIPT system subject to channel estimation errors, offering a more practical design perspective.

References

[1] F. Liu, Y. Cui, C. Masouros, J. Xu, T. X. Han, Y. C. Eldar, and S. Buzzi, "Integrated sensing and communications: Toward dual-functional wireless networks for 6G and beyond," *IEEE J. Sel. Areas Commun.*, vol. 40, no. 6, pp. 1728–1767, Mar. 2022.

[2] F. Liu, C. Masouros, A. Li, T. Ratnarajah, and J. Zhou, "MIMO radar and cellular coexistence: A power-efficient approach enabled by interference exploitation," *IEEE Trans. Signal Process.*, vol. 66, no. 14, pp. 3681–3695, Jul. 2018.

[3] Z. Wei, H. Qu, Y. Wang, X. Yuan, H. Wu, Y. Du, K. Han, N. Zhang, and Z. Feng, "Integrated sensing and communication signals toward 5g-a and 6g: A survey," *IEEE Internet Things J.*, vol. 10, no. 13, pp. 11 068–11 092, Jul. 2023.

[4] X. Cheng, D. Duan, S. Gao, and L. Yang, "Integrated sensing and communications (isac) for vehicular communication networks (vcn)," *IEEE Internet Things J.*, vol. 9, no. 23, pp. 23 441–23 451, Dec. 2022.

[5] Q. Wu and R. Zhang, "Intelligent reflecting surface enhanced wireless network via joint active and passive beamforming," *IEEE Trans. Wireless Commun.*, vol. 18, no. 11, pp. 5394–5409, Nov. 2019.

[6] W. Saad, M. Bennis, and M. Chen, "A vision of 6G wireless systems: Applications, trends, technologies, and open research problems," *IEEE Network*, vol. 34, no. 3, pp. 134–142, Jun. 2020.

[7] N. Shlezinger, G. C. Alexandropoulos, M. F. Imani, Y. C. Eldar, and D. R. Smith, "Dynamic metasurface antennas for 6G extreme massive MIMO communications," *IEEE Wireless Commun.*, vol. 28, no. 2, pp. 106–113, Apr. 2021.

[8] C. Pan, H. Ren, K. Wang, M. Elkashlan, A. Nallanathan, J. Wang, and L. Hanzo, "Intelligent reflecting surface aided MIMO broadcasting for simultaneous wireless information and power transfer," *IEEE J. Sel. Areas Commun.*, vol. 38, no. 8, pp. 1719–1734, Aug. 2020.

[9] Z. Yang and Y. Zhang, "Beamforming optimization for RIS-aided SWIPT in cell-free MIMO networks," *China Communications*, vol. 18, no. 9, pp. 175–191, Sep. 2021.

[10] Y. Zeng, B. Clerckx, and R. Zhang, "Communications and signals design for wireless power transmission," *IEEE Trans. Commun.*, vol. 65, no. 5, pp. 2264–2290, May. 2017.

[11] B. Clerckx, R. Zhang, R. Schober, D. W. K. Ng, D. I. Kim, and H. V. Poor, "Fundamentals of wireless information and power transfer: From RF energy harvester models to signal and system designs," *IEEE J. Sel. Areas Commun*, vol. 37, no. 1, pp. 4–33, Jan. 2019.

[12] S. Pala, M. Katwe, K. Singh, T. A. Tsiftsis, and C.-P. Li, "Robust transmission design for RIS-aided full-duplex-RSMA V2X communications via multi-agent DRL," *IEEE Trans. Veh. Technol.*, pp. 1–15, 2024.

[13] S. Pala, P. Saikia, S. K. Singh, K. Singh, and C.-P. Li, "Design of RIS-assisted full duplex 6G-V2X communications," in *IEEE WCNC*, Mar. 2023, pp. 1–6.

[14] P. Saikia, K. Singh, S. K. Singh, W.-J. Huang, C.-P. Li, and S. Biswas, "Beamforming design in vehicular communication systems with multiple reconfigurable intelligent surfaces: A deep learning approach," *IEEE Access*, vol. 11, pp. 100 832–100 844, Sep. 2023.

[15] J. Yaswanth, M. Katwe, K. Singh, S. Prakriya, and C. Pan, "Robust beamforming design for active-RIS aided MIMO SWIPT communication system: A power minimization approach," *IEEE Trans. Wireless Commun.*, vol. 23, no. 5, pp. 4767–4785, May. 2024.

[16] Q. Zhu, M. Li, R. Liu, and Q. Liu, "Cramér-rao bound optimization for active RIS-empowered ISAC systems," *IEEE Trans. Wireless Commun.*, vol. 23, no. 9, pp. 11 723–11 736, 2024.

[17] S. Singh, A. Raviteja, K. Singh, S. K. Singh, A. Kaushik, and M.-L. Ku, "Secrecy rate maximization for active RIS-aided robust uplink NOMA communications," *IEEE Wireless Commun. Lett.*, pp. 1–1, Jul. 2024.

[18] A. A. Salem, M. H. Ismail, and A. S. Ibrahim, "Active reconfigurable intelligent surface-assisted MISO integrated sensing and communication systems for secure operation," *IEEE Trans. Veh. Technol.*, vol. 72, no. 4, pp. 4919–4931, Apr. 2023.

[19] J. Yaswanth, M. Katwe, K. Singh, O. Taghizadeh, C. Pan, and A. Schmeink, "Towards green communication: Power-efficient beamforming for STAR-RIS-aided SWIPT," *IEEE Trans. Green Commun. Netw.*, pp. 1–1, Feb. 2024.

[20] P. Saikia, A. Jee, K. Singh, C. Pan, T. A. Tsiftsis, and W.-J. Huang, "RIS-aided integrated sensing and communications," in *IEEE GLOBECOM*, Dec. 2023, pp. 5080–5085.

[21] Z. Yang, S. Zhang, G. Chen, Z. Dong, Y. Wu, and D. Benevides da Costa, "Secure integrated sensing and communication systems assisted by active RIS," *IEEE Transactions on Vehicular Technology*, vol. 73, no. 12, pp. 19 791–19 796, 2024.

[22] S. Fang, G. Chen, P. Xiao, K.-K. Wong, and R. Tafazolli, "Intelligent omni surface-assisted self-interference cancellation for full-duplex MISO system," *IEEE Transactions on Wireless Communications*, vol. 23, no. 3, pp. 2268–2281, 2024.

[23] S. Fang, G. Chen, Z. Abdullah, and Y. Li, "Intelligent omni surface-assisted secure mimo communication networks with artificial noise," *IEEE Communications Letters*, vol. 26, no. 6, pp. 1231–1235, 2022.

[24] W. Du and *et al.*, "STAR-RIS assisted wireless powered IoT networks," *IEEE Trans. Veh. Tech.*, 2023.

[25] H. R. Hashempour, H. Bastami, M. Moradikia, S. A. Zekavat, H. Behroozi, and A. L. Swindlehurst, "Secure SWIPT in STAR-RIS aided downlink MISO rate-splitting multiple access networks," *arXiv preprint arXiv:2211.09081*, 2022.

[26] J. Zuo and Y. Liu, "Reconfigurable intelligent surface assisted NOMA empowered integrated sensing and communication," in *IEEE GC Wkshps*, Jan. 2022, pp. 1028–1033.

[27] C. Pan, H. Ren, K. Wang, W. Xu, M. Elkashlan, A. Nallanathan, and L. Hanzo, "Multicell MIMO communications relying on intelligent reflecting surfaces," *IEEE Trans. Wireless Commun.*, vol. 19, no. 8, pp. 5218–5233, May. 2020.

[28] Q. Zhu, M. Li, R. Liu, Y. Liu, and Q. Liu, "Joint beamforming designs for active reconfigurable intelligent surface: A sub-connected array architecture," *IEEE Transactions on Communications*, vol. 70, no. 11, pp. 7628–7643, 2022.

[29] M. Bian, Y. Shi, Y. Huang, and X.-W. Tang, "QoS-aware energy storage maximization in the RIS-aided joint-SWIPT-MEC system," *IEEE Commun. Lett.*, vol. 27, no. 12, pp. 3434–3438, Dec. 2023.

[30] Z. Zhou, X. Li, G. Zhu, J. Xu, K. Huang, and S. Cui, "Integrating sensing, communication, and power transfer: Multiuser beamforming design," *IEEE J. Sel Areas Commun.*, vol. 42, no. 9, pp. 2228–2242, 2024.

[31] Y. Chen, H. Hua, J. Xu, and D. W. K. Ng, "ISAC meets SWIPT: Multi-functional wireless systems integrating sensing, communication, and powering," *IEEE Trans. Wireless Commun.*, vol. 23, no. 8, pp. 8264–8280, 2024.

[32] X. Li, Z. Han, G. Zhu, Y. Shi, J. Xu, Y. Gong, Q. Zhang, K. Huang, and K. B. Letaief, "Integrating sensing, communication, and power transfer: From theory to practice," *IEEE Commun. Mag.*, vol. 62, no. 9, pp. 122–127, 2024.

[33] Y. Chen, H. Hua, and J. Xu, "Transmit optimization for multi-functional MIMO systems integrating sensing, communication, and powering," in *IEEE ICC*, Jun. 2023, pp. 1518–1523.

[34] K.-H. Park, M.-S. Alouini, and Y. Chen, "Throughput-maximized network deployment in a multi-NIB-aided ISAC network," in *IEEE GC Wkshps*, Dec. 2023, pp. 1410–1415.

[35] M. Liu and M. Yang, "Performance analysis of SWIPT assisted NO-DLT ISAC systems," in *IEEE PIMRC*, Sep. 2023, pp. 1–6.

[36] J. Chu, Z. Lu, R. Liu, M. Li, and Q. Liu, "Joint beamforming and reflection design for secure RIS-ISAC systems," *IEEE Trans. Veh. Technol.*, vol. 73, no. 3, pp. 4471–4475, Mar. 2024.

[37] M. Hua, Q. Wu, C. He, S. Ma, and W. Chen, "Joint active and passive beamforming design for IRS-aided radar-communication," *IEEE Trans. Wireless Commun.*, vol. 22, no. 4, pp. 2278–2294, Apr. 2023.

[38] R. S. P. Sankar, S. P. Chepuri, and Y. C. Eldar, "Beamforming in integrated sensing and communication systems with reconfigurable intelligent surfaces," *IEEE Trans. Wireless Commun.*, vol. 23, no. 5, pp. 4017–4031, May. 2024.

[39] Z. Xing, R. Wang, and X. Yuan, "Joint active and passive beamforming design for reconfigurable intelligent surface enabled integrated sensing and communication," *IEEE Trans. Commun.*, vol. 71, no. 4, pp. 2457–2474, Apr. 2023.

[40] R. Liu, M. Li, H. Luo, Q. Liu, and A. L. Swindlehurst, "Integrated sensing and communication with reconfigurable intelligent surfaces: Opportunities, applications, and future directions," *IEEE Wireless Commun.*, vol. 30, no. 1, pp. 50–57, Feb. 2023.

[41] S. P. Chepuri, N. Shlezinger, F. Liu, G. C. Alexandropoulos, S. Buzzi, and Y. C. Eldar, "Integrated sensing and communications with reconfigurable intelligent surfaces: From signal modeling to processing," *IEEE Signal Process. Mag.*, vol. 40, no. 6, pp. 41–62, Sep. 2023.

[42] R. Allu, M. Katwe, K. Singh, T. Q. Duong, and C.-P. Li, "Robust energy efficient beamforming design for ISAC full-duplex communication systems," *IEEE Wireless Communications Letters*, vol. 13, no. 9, pp. 2452–2456, 2024.

[43] K. Xie, G. Cai, J. He, and G. Kaddoum, "STAR-RIS aided MISO SWIPT-NOMA system with energy buffer: Performance analysis and optimization," *arXiv preprint arXiv:2308.09489*, 2023.

[44] X. Mu, Y. Liu, L. Guo, J. Lin, and R. Schober, "Simultaneously transmitting and reflecting (STAR) RIS aided wireless communications," *IEEE Trans. Wireless Commun.*, vol. 21, no. 5, pp. 3083–3098, Oct. 2021.

[45] J. Xu, Y. Liu, X. Mu, and O. A. Dobre, "STAR-RISs: Simultaneous transmitting and reflecting reconfigurable intelligent surfaces," *IEEE Commun. Lett.*, vol. 25, no. 9, pp. 3134–3138, Sep. 2021.

[46] R. Long, Y.-C. Liang, Y. Pei, and E. G. Larsson, "Active reconfigurable intelligent surface-aided wireless communications," *IEEE Trans. Wireless Commun.*, vol. 20, no. 8, pp. 4962–4975, Mar. 2021.

[47] R. Zhang and C. K. Ho, "MIMO broadcasting for simultaneous wireless information and power transfer," *IEEE Trans. Wireless Commun.*, vol. 12, no. 5, pp. 1989–2001, May. 2013.

[48] Y. Fang, Y. Tao, H. Ma, Y. Li, and M. Guizani, "Design of a reconfigurable intelligent surface-assisted FM-DCSK-SWIPT scheme with nonlinear energy harvesting model," *arXiv preprint arXiv:2205.06971*, Oct. 2022.

[49] H. Luo, R. Liu, M. Li, and Q. Liu, "RIS-aided integrated sensing and communication: Joint beamforming and reflection design," *IEEE Trans. Veh. Tech.*, Feb. 2023.

[50] C. Pan, H. Ren, M. Elkashlan, A. Nallanathan, and L. Hanzo, "Robust beamforming design for ultra-dense user-centric C-RAN in the face of realistic pilot contamination and limited feedback," *IEEE Trans. Wireless Commun.*, vol. 18, no. 2, pp. 780–795, Dec 2019.

[51] M. Grant and S. Boyd, "CVX: Matlab software for disciplined convex programming, version 2.1," http://cvxr.com/cvx, Mar. 2014.

[52] X.-D. Zhang, *Introduction to Matrix Algebra*. Cambridge University Press, 2017, p. 3–94.

[53] C. Pan, H. Ren, M. Elkashlan, A. Nallanathan, and L. Hanzo, "The noncoherent ultra-dense C-RAN is capable of outperforming its coherent counterpart at a limited fronthaul capacity," *IEEE J. Sel. Areas Commun.*, vol. 36, no. 11, pp. 2549–2560, Nov. 2018.

[54] Y. Sun, P. Babu, and D. P. Palomar, "Majorization-minimization algorithms in signal processing, communications, and machine learning," *IEEE Trans. Signal Processing*, vol. 65, no. 3, pp. 794–816, Feb. 2016.

[55] G. Zheng, "Joint beamforming optimization and power control for full-duplex MIMO two-way relay channel," *IEEE Trans. Signal Process.*, vol. 63, no. 3, pp. 555–566, Dec. 2014.

Jetti Yaswanth received a bachelor's degree in Electronics and Communication Engineering from the Swarnandhra College of Engineering and Technology, Andhra Pradesh, India, in 2020, and Master of Science degree with the International Master's Program in Telecommunication Engineering, Institute of Communications Engineering from National Sun Yat-sen University (NSYSU), Kaohsiung, Taiwan in 2023. He is currently with Whetron Electronics CO., LTD. to develop ADAS technology for automobiles. His interests include multi-input multi-output, reconfigurable intelligent surface, NOMA, SWIPT, energy harvesting, machine learning and Advanced-driverless Assistance Systems.

Prajwalita Saikia (**Member, IEEE**) received her M.Sc. degree in Electronics and Communication Technology from Gauhati University, Assam, India in 2018, M.Tech degree in Electronics and Communication Engineering from Indian Institute of Information Technology Guwahati (IIITG), Assam, India in 2021, and Ph.D. degree in Communication Engineering from the Institute of Communications Engineering, National Sun Yat-Sen University, Taiwan in 2024. She is currently a Postdoctoral Research Fellow at University College Dublin, Ireland. Her current research interests include integrated sensing and communication, reconfigurable intelligent surface assisted communications, V2X communications, full duplex communications, machine learning for wireless communications. She has been a reviewer of reputed journals, such as IEEE TWC, IEEE TGCN, IEEE WCL.

Keshav Singh (Member, IEEE) received the Ph.D. degree in Communication Engineering from National Central University, Taiwan, in 2015. He is currently with the Institute of Communications Engineering, National Sun Yat-sen University (NSYSU), Taiwan, as an Associate Professor. He is also also with the Department of Electronic Engineering, Kyung Hee University, Yongin-si, Gyeonggi-do 17104, South Korea. Prior to this, he held the position of Research Associate from 2016 to 2019 at the Institute of Digital Communications, University of Edinburgh, U.K. From 2019 to 2020, he was associated with the University College Dublin, Ireland, as a Research Fellow. He leads research in the areas of transceiver design for full-duplex radio, machine learning for wireless communications, integrated sensing and communications, non-terrestrial networks, and large intelligent surface-assisted communications.

Dr. Singh chaired workshops on conferences like IEEE GLOBECOM 2023 and IEEE WCNC 2024. He also serves/served as leading guest editor for IEEE Transactions on Green Communications and Networking Special Issue on Design of Green Near-Field Wireless Communication Networks and IEEE Internet-of-Things Journal Special Issue on Positioning and Sensing for Near-Filed (NF)-driven Internet-of-Everything. He is also an Associate Editor of IEEE Communications Surveys & Tutorials.

Yun Hee Kim (S'97-M'00-SM'05) received the B.S.E. (*summa cum laude*), M.S.E., and Ph.D. degrees in electrical engineering from Korea Advanced Institute of Science and Technology, Daejeon, Korea, in 1995, 1997, and 2000, respectively. She was with the Electronics and Telecommunications Research Institute, Daejeon, Korea, as a Senior Research Staff from 2000 to 2004. In 2004, she joined Kyung Hee University, Yongin, Korea, where she is currently a Professor in the department of Electronic Engineering. In 2000 and 2011, she was a Visiting Researcher at the University of California, San Diego (UCSD), La Jolla, CA, USA. Her research interests include wireless communication, signal processing, and artificial intelligence.

Prof. Kim has served as a member of the technical program committee of numerous conferences including IEEE Vehicular Technology Conference and Global Communications Conference. She is a Senior Member of the IEEE, and was recognized as one of the ten N2Women Stars in Networking and Communications in 2024. Currently, she is an Associate Editor of IEEE Wireless Communications Letters, Journal of Communications and Networks (JCN), and ICT Express.

Trung Q. Duong (Fellow, IEEE) is a Canada Excellence Research Chair (CERC) and a Full Professor at Memorial University, Canada. He is also an adjunct professor at Queen's University Belfast, UK, a visiting professor at Kyung Hee University, South Korea, and an adjunct professor at Duy Tan University, Vietnam. His current research interests include wireless communications, quantum machine learning, and quantum optimization.

He is the Editor-in-Chief of IEEE Communications Surveys & Tutorials. He has received two prestigious awards from the Royal Academy of Engineering (RAEng): RAEng Research Chair in 2020 and RAEng Research Fellow in 2015. He was awarded the prestigious Newton Prize in 2017. He is a Fellow of the Engineering Institute of Canada (EIC) and Asia-Pacific Artificial Intelligence Association (AAIA).